JGR Oceans

RESEARCH ARTICLE
10.1029/2024JC021237

Special Collection:
The Arctic Ocean's changing Beaufort Gyre

Simulated Impact of Time-Varying River Runoff and Greenland Freshwater Discharge on Sea Level Variability in the Beaufort Gyre Over 2005–2018

S. Tajouri[1], W. Llovel[1], F. Sévellec[1,2], J.-M. Molines[3], P. Mathiot[3], T. Penduff[3], and S. Leroux[4]

[1]Laboratoire d'Océanographie Physique et Spatiale (LOPS), University Brest, CNRS, IRD, IFREMER, Plouzané, France, [2]Odyssey Team-Project, INRIA CNRS, Brest, France, [3]Université Grenoble Alpes, CNRS, INRAE, IRD, Grenoble INP, Institut des Géosciences de l'Environnement (IGE), Grenoble, France, [4]Datlas, Grenoble, France

Abstract Global mean sea level has been rising at a rate of 3.25 ± 0.4 mm yr^{-1} over 1993–2018. Yet several regions are increasing at a much faster rate, such as the Beaufort Gyre in the Arctic Ocean at a rate of 9.3 ± 7.0 mm yr^{-1} over 2003–2014. At interannual to decadal time scales, the Beaufort Gyre sea level is controlled by salinity changes due to sea ice melt and wind-driven lateral Ekman convergence–divergence of freshwater. This study uses recent Greenland discharge and river runoff estimates to isolate and quantify the sea level response to freshwater fluxes variability over the period 1980–2018. It relies on sensitivity experiments based on a global ocean model including sea-ice and icebergs. These sensitivity experiments only differ by the freshwater fluxes temporal variability of Greenland and global rivers which are either seasonal climatologies or fully time varying, revealing the individual and combined impact of these freshwater sources fluctuations. Fully varying Greenland discharge and river runoff produce an opposite impact on sea level trends over 2005–2018 in the Beaufort Gyre region, the former driving an increase, while the latter, a decrease. Their combined impact leads to a fairly weak sea level trend. The sea level response is primarily driven by salinity variations in the upper 300 m, which are mainly caused by salinity advection involving complex compensations between passive, active, and nonlinear advection. This study shows that including the temporal variability of freshwater fluxes in forced global ocean models results in a better representation of regional sea level change.

Plain Language Summary Sea level is rising globally but not at the same rate everywhere. In the Arctic Ocean, the Beaufort Gyre sea level has been increasing at a fast rate of 9.3 ± 7.0 mm yr^{-1} over 2003–2014. At long time scales, the Beaufort Gyre sea level change is controlled by salinity, which depends mainly on continental freshwater runoff—particularly high in this region—and sea ice melt. This study uses recent estimates of Greenland discharge and river runoff in a global ocean model. The aim is to isolate and quantify the sea level response of the Beaufort Gyre to freshwater fluxes variability. We compare numerical simulations where Greenland discharge and river runoff are fully varying or set to a repeated seasonal cycle to reveal the individual and combined impacts of the variability of these freshwater sources on regional sea level. Both Greenland discharge and global river runoff impact remotely the Beaufort Gyre sea level. They induce salinity variations in the upper 300 m of the gyre through salinity advection. This study highlights the importance of the variability of continental freshwater fluxes in models in order to better represent regional sea level variability.

Key Points:

- Greenland discharge and river runoff variability contribute to sea level rise and fall in the Beaufort Gyre
- The positive impact of Greenland is greater than the negative impact of rivers in the 0–78-m range, and vice versa in the 78–300-m range
- Sea level change in the sensitivity experiments is mostly halosteric with salinity changes mainly controlled by advection

Supporting Information:

Supporting Information may be found in the online version of this article.

Correspondence to:

S. Tajouri,
soumaia.tajouri@ifremer.fr

Citation:

Tajouri, S., Llovel, W., Sévellec, F., Molines, J.-M., Mathiot, P., Penduff, T., & Leroux, S. (2024). Simulated impact of time-varying river runoff and Greenland freshwater discharge on sea level variability in the Beaufort Gyre over 2005–2018. *Journal of Geophysical Research: Oceans*, *129*, e2024JC021237. https://doi.org/10.1029/2024JC021237

Received 17 APR 2024
Accepted 12 AUG 2024

Author Contributions:

Conceptualization: S. Tajouri, W. Llovel, F. Sévellec
Data curation: J.-M. Molines, P. Mathiot, S. Leroux
Formal analysis: S. Tajouri
Funding acquisition: W. Llovel, T. Penduff
Investigation: S. Tajouri
Methodology: S. Tajouri, W. Llovel, F. Sévellec

1. Introduction

Global mean sea level (GMSL) is an integrative indicator of climate change. GMSL has been routinely measured by satellite altimetry since 1992. GMSL rise is due to global ocean warming, ocean mass increase from melting of continental glaciers and ice sheets, and changes in land water storage (Chen et al., 2017; Llovel et al., 2023). Altimetry data has revealed a linear trend of 3.25 ± 0.4 mm yr^{-1} over 1993–2018 and 3.69 ± 0.5 mm yr^{-1} over 2006–2018 (Fox-Kemper et al., 2021) suggesting an acceleration over the entire altimetric period (Nerem et al., 2018). This acceleration is attributed to an increased ice-sheet mass loss (Fox-Kemper et al., 2021). Moreover, satellite altimetry has revealed large regional variability in sea level trends with regions experiencing trends three times as large as the global mean trend. Among other drivers, these regional sea level changes can be driven by density changes known as steric sea level changes (Stammer et al., 2013). Thermosteric and halosteric sea level correspond to the parts of the steric sea level associated with temperature and salinity changes, respectively. Evaluating and understanding regional sea level rise is crucial for society as it would be helpful for

Project administration: W. Llovel, T. Penduff
Resources: J.-M. Molines, S. Leroux
Software: S. Tajouri, J.-M. Molines, S. Leroux
Supervision: W. Llovel, F. Sévellec
Validation: S. Tajouri
Visualization: S. Tajouri
Writing – original draft: S. Tajouri
Writing – review & editing: S. Tajouri, W. Llovel, F. Sévellec

adaptation and/or mitigation efforts for enhanced flooding, salt water intrusion, erosion, and storm surges (Moftakhari et al., 2015; Neumann et al., 2015; Proshutinsky et al., 2004).

Satellite altimetry data has revealed a positive sea level trend over the Arctic Ocean (66°N to 82°N) of 2.2 ± 1.2 mm yr^{-1} since the 1990s (Armitage et al., 2016; Cheng et al., 2015; Fu et al., 2021; Rose et al., 2019). The greatest rate of sea level rise (15 mm yr^{-1}) is found in the Beaufort Gyre Region (BGR) in the Canada Basin (Figure S1 in Supporting Information S1 highlights the main Arctic features). This rise has a halosteric origin due to freshwater content increase (Carret et al., 2017; Fukumori et al., 2021; Raj et al., 2020). The anticyclonic Beaufort Gyre is the Arctic Ocean largest freshwater reservoir. The Beaufort Gyre is the main feature of the Arctic sea level and is characterized by a doming of the mean dynamic height. Its circulation and sea level fluctuation are related to two main atmospheric circulation regimes over the Arctic Ocean. When the Beaufort High atmospheric pressure—an anticyclonic circulation over the Canadian sector—dominates, the Beaufort Gyre accumulates freshwater by Ekman convergence in the surface ocean layer. Whereas an Icelandic Low pressure system—a cyclonic regime–results in the release of freshwater from the Beaufort Gyre by Ekman divergence (M. Timmermans & Marshall, 2020). The Arctic Ocean has been under an anticyclonic atmospheric circulation regime since 1997 leading to BGR freshwater content increase causing halosteric changes in sea level (Andersen & Piccioni, 2016; Armitage et al., 2016; Carret et al., 2017; Giles et al., 2012; Jin et al., 2023; Ludwigsen et al., 2022; Proshutinsky et al., 2009, 2015; Regan et al., 2019; Rose et al., 2019). The continuously increasing freshwater input from Greenland into the north Atlantic subpolar region has been hypothesized as a major explanation for the cessation of the decadal variability of the Gyre circulation since the late 1990s (Proshutinsky et al., 2015).

Models and reanalysis studies have been widely used to estimate the freshwater budget of the Arctic Ocean and to understand the origin of the freshwater accumulating in the BGR. On interannual timescales, it can originate from sea ice melt, the Eurasian runoff, the Mackenzie River runoff, and the Bering strait transport (Fukumori et al., 2021; Kelly et al., 2019; Morison et al., 2012; Proshutinsky et al., 2019). Jahn et al. (2012) compared the freshwater budget in 10 forced ocean-sea ice simulations, and found that most of their differences were related to the interannual variability of the liquid freshwater export, especially through Fram Strait, and to the liquid freshwater storage in the Arctic due to differences in the salinity field. Therefore, they pointed out the need to improve the simulations by better representing the variability of the salinity field in the Arctic. Thus, to reduce the uncertainties, it is necessary to identify the mechanisms and quantify the individual contributors to salinity variability. Here, we focus our attention on the impact of the temporal variability of river runoff and Greenland discharge.

Temporal variations in river runoff potentially affect the salinity field in the Arctic, yet forced models commonly use seasonal runoff climatology as forcing. Greenland's freshwater fluxes, if included, are rarely realistically represented in their space-time variability. The sensitivity of the Arctic salinity field in models to the variability of freshwater input from rivers and Greenland is largely unknown. The increasing melting of Greenland since the mid-1990s has been a new phenomenon in the climate system. Recent improvements in the estimation of Greenland mass loss, both solid and liquid (Mouginot et al., 2019), and river runoff (from Land Surface Model outputs) (Decharme et al., 2019) allow us to isolate and quantify the sea level response to these freshwater fluxes variability. To do so, we use ocean sensitivity simulations implemented in a 1/4° global ocean general circulation model, which includes sea-ice and icebergs, integrated over the 1980–2018 period. The goal of the present study is to assess the impact of Greenland's melting and global river runoff spatiotemporal variability on regional sea level trends in the Beaufort Gyre over the 2005–2018 period and to understand the related mechanisms.

The paper is organized as follows. In Section 2, we describe the model, the data sets used for model evaluation, and the methods. We evaluate the simulations in Section 3.1. In Section 3.2, we characterize the effects of freshwater fluxes variability on sea level and its components. In Section 3.3, we analyze salinity budgets to assess the physical processes involved. We finally discuss our results in Section 4 and conclude in Section 5.

2. Data Sets and Methods

2.1. Model Simulations

The Nucleus for European Modeling of the Ocean (NEMO) model version 4.0 (Madec et al., 2019) is used in a global configuration at 0.25° horizontal resolution (around 10 km in the Arctic). This configuration includes sea-ice and icebergs. There are 75 vertical levels of decreasing resolution from 1 m at the surface to 200 m at the

bottom, including 24 levels within the upper 100 m. The vertical coordinate uses a partial step formulation to accommodate the bottom topography (Barnier et al., 2006). The model uses a non-linear free surface, meaning that the thickness of each vertical level varies at each time step. At the surface, the model is forced by the JRA-55 atmospheric reanalysis at a 3-hr resolution (Kobayashi et al., 2015) using the National Center for Atmospheric Research (NCAR) bulk formulae (Large & Yeager, 2004). NEMO is fully coupled with the sea ice model SI3 (Vancoppenolle et al., 2023). SI3 represents sea ice as levitating over the ocean, hence sea ice does not apply any mass loading effect at the surface. It is exchanging heat, salt, mass, and momentum with the ocean.

A first simulation was produced from 1 January 1958 to 31 December 2019 starting from rest, using as initial conditions the world ocean atlas (WOA18) temperature and salinity (Garcia et al., 2019). This first simulation uses climatological (i.e., a repeated seasonal cycle) runoff and discharge everywhere. To avoid any spurious salinity drift due to the fact that the model is not coupled with the atmosphere, the sea surface salinity (SSS) in this first simulation is relaxed toward the WOA18 monthly climatology (Garcia et al., 2019) with a time scale of 60 days applied to a surface layer of 10 m. The model SSS is spatially smoothed before computing the model/climatology mismatch to restore only the large-scale features. From 150 km heading toward the coastline, the SSS restoring is progressively reduced to zero at the coast using a smooth transition (hyperbolic tangent) to allow the modeled coastal current systems to carry freshwater of continental origin. In this first simulation, the SSS relaxation term was stored monthly, and converted into a freshwater air-sea flux correction term for our actual sensitivity experiments where no SSS relaxation was applied. This strategy ensures that SSS freely evolves in the sensitivity experiments with no risk of unrealistic trends in salinity or sea level. The three sensitivity experiments were initialized from a restart file of the first simulation on 1 January 1980 and ran until 31 December 2018. They are forced at the surface by the fully varying JRA-55 forcing with the freshwater air-sea flux correction described above.

In NEMO, the continental freshwater fluxes are of four kinds: surface runoff, subglacial runoff, iceberg melting, and ice shelf melting. First, river runoff is spread over the top 10 m of the ocean. Second, Greenland ice sheet freshwater fluxes come from multiple sources. The surface runoff from land terminating glaciers is routed to the closest NEMO coastal wet cell and treated as river runoff. The subglacial runoff from marine terminating glaciers is routed to the NEMO coastal wet cell near the mouth of the fjord and then spread between the surface and the fjord's sill depth (the maximum is 720 m, Figure S2 in Supporting Information S1). This method is a good approximation of what has been observed in the Jakobshavn Fjord (Gladish et al., 2015). Calving from the tide water glacier is translated to the model fjord mouth. Because of the melting of icebergs in the fjords, 50% of the iceberg mass is converted to liquid discharge at the first model sea-point (Enderlin et al., 2016), and treated together with subglacial runoff. The remaining 50% are kept to feed as calving source the explicit iceberg representation (using the Lagrangian iceberg model of Marsh et al. (2015)). Thirdly, Antarctica's freshwater fluxes are represented as iceberg and ice shelf melting. More details about the implementation of Antarctica's and Greenland's freshwater fluxes are given in the Figure S2 of Supporting Information S1.

The fully varying and seasonal climatological freshwater fluxes used to force our sensitivity simulations were derived from three data sets. The fully varying daily river runoff and daily climatology over 1979–2018 come from the ISBA-CTRIP land surface model-reanalysis (Decharme et al., 2019). This data set was validated in the Arctic Ocean against stations in the polar basins: Mackenzie, Ob, and Lena from 1979 to 2010 (Decharme et al., 2019, their Figure 14 and Table 4). Mouginot et al. (2019) provided the fully varying Greenland mass loss monthly data (both solid and liquid). The monthly climatology of Greenland's discharge was estimated over 1950–1972, corresponding to the period prior to Greenland's current intense melting trend (Mouginot et al., 2019). For Antarctica, the annual calving and basal melt rates estimates for each ice shelf were derived from Rignot et al. (2013), and they do not vary between simulations. Taking into account the full temporal variability of river runoff and Greenland discharge–including trends–represents a real change from the commonly applied repeated seasonal cycle.

The sensitivity simulations aim at assessing the impact of the fully varying freshwater fluxes from Greenland and rivers on regional sea level change. The reference simulation (exp1) corresponds to all continental fluxes set as fully varying (except Antarctica). The second experiment (exp2) corresponds to all rivers set as fully varying and Greenland's discharge set as seasonal. The third experiment (CLIM) corresponds to all continental fluxes set as seasonal. The difference exp1 − exp2 is interpreted as the impact of Greenland fully varying discharge (referred to as GREENLAND hereafter). Similarly, the difference exp2 − CLIM is interpreted as the impact of fully

varying river runoff (referred to as RIVERS hereafter). The difference exp1 − CLIM is interpreted as the combined impact of fully varying Greenland discharge and river runoff (referred to as Gr + Riv hereafter). Following the definitions of the experiments, we have Gr + Riv = GREENLAND + RIVERS.

2.2. Data Sets Used for Model Evaluation

To evaluate exp1, we compare the sea level anomalies (SLA) of exp1 with the SLA of five altimetry-derived data sets in the BGR. These products are different since specific processing and corrections are applied to the ice-covered Arctic region and the time coverage of each of them is different, as they rely on different combinations of satellites. We use the version 3.1 of the Climate Change Initiative (CCI) Technical University of Denmark (DTU) monthly Arctic SLA based on ERS-1/-2, Envisat, and CryoSat-2 satellites, spanning September 1991 to September 2018 (Rose et al., 2019). The monthly Arctic dynamic topography data set (Armitage et al., 2016, 2017) spans over the 2003–2014 period and is based on Envisat and CryoSat-2. The Center for Polar Observation and Modeling (CPOM) data set (www.cpom.ucl.ac.uk/dynamic_topography) and the data set of Doglioni et al. (2021) are both based solely on CryoSat-2 and span the 2011–2020 period. Finally, we use the Delayed-Time Level-4 sea surface height experimental product of Prandi et al. (2021) which combines three missions (SARAL/AltiKa, CryoSat-2, and Sentinel-3A) and has been providing one gridded field every 3 days since 2011.

We also consider the ECCO Version 4 Release 4 (ECCO V4r4) output (ECCO Consortium et al., 2021b). ECCO V4r4 is an ocean-sea ice state estimate using the Massachusetts Institute of Technology general circulation model (MITgcm) (Marshall et al., 1997) coupled with a prognostic dynamic and thermodynamic sea ice model (Losch et al., 2010). The model is constrained by almost every available data over the ocean during the 1992–2017 period (ECCO Consortium et al., 2021b). ECCO V4r4 is physically consistent which enables the investigation of the physical mechanisms governing the ocean (Forget et al., 2015). ECCO V4r4 spans from 1992 to 2017 and uses a non-linear free-surface formulation and real freshwater flux boundary condition (Campin et al., 2008; Fukumori et al., 2021). In contrast to our simulations, ECCO V4r4 sea-ice model accounts for the mass loading effect of sea-ice on sea level (Forget et al., 2015).

2.3. Sea Level Change Framework

The expression of sea level comes from the hydrostatic balance (Gill & Niller, 1973). By integrating the hydrostatic equation from the sea surface (η) down to the bottom of the ocean ($-h$), and by removing the temporal mean computed over the entire period, the ocean surface elevation, also called sea level anomaly (η'), can be written as follows:

$$\eta' = \underbrace{-\frac{1}{\rho_0}\int_{-h}^{0} \rho' \, dz}_{steric} + \underbrace{\frac{P'_b - P'_a}{\rho_0 g}}_{manometric}, \tag{1}$$

where z is the vertical coordinate, P'_a the deviation of the sea-surface loading (such as atmospheric surface pressure) from its temporal mean, ρ_0 the mean seawater density (1026 kg m^{-3} in NEMO), g the acceleration of gravity, ρ' the density deviation from its temporal mean, and P'_b the bottom pressure deviation from its temporal mean. The terms of the right-hand side of Equation 1 correspond to the steric SLA and the manometric SLA which is associated with mass changes (Gregory et al., 2019). In NEMO, the atmospheric surface pressure and the sea ice loading effect are neglected leading to no sea-surface loading.

As the model is based on the Boussinesq approximation, the global mean steric sea level is not explicitly represented (Greatbatch, 1994). The GMSL (corresponding to the barystatic sea level) is subtracted at each time step in each simulation. The model SLA evolution reflects changes in ocean volume due to ocean density and mass changes. Taking the time derivative of Equation 1, the SLA tendency equation can be written at each grid point as follows:

$$\frac{\partial \eta'}{\partial t} = -\frac{1}{\rho_0}\int_{-h}^{0} \frac{\partial \rho'(T,S,p)}{\partial t} \, dz + \frac{1}{\rho_0 g}\frac{\partial P'_b}{\partial t}, \tag{2}$$

where t is time and T, S, and p are temperature, salinity, and pressure, respectively. Thus, the first term in Equation 2 reflects the contribution to sea level change of local changes in density (steric sea level) and the second term reflects the contribution of the local mass change (manometric sea level) (Gregory et al., 2019). Manometric sea level trend is obtained at each grid point by subtracting the steric sea level trend from the SLA trend. As seawater density changes are driven by temperature and salinity changes, steric sea level changes can be further decomposed into temperature change (thermosteric sea level η'_{thermo}) and salinity change (halosteric sea level η'_{halo}) contributions. Their vertically integrated trends have been computed from the surface to any depth level k as follows:

$$\frac{\partial \eta'_{\text{thermo}}}{\partial t} = \frac{1}{\rho_0}\int_{-k}^{0} \frac{\partial \rho'\left(T,\overline{S},p\right)}{\partial t}\, dz, \tag{3}$$

$$\frac{\partial \eta'_{\text{halo}}}{\partial t} = \frac{1}{\rho_0}\int_{-k}^{0} \frac{\partial \rho'\left(\overline{T},S,p\right)}{\partial t}\, dz, \tag{4}$$

where the overbars indicate the time-mean over the 1980–2018 period.

2.4. Salinity Budget of the Beaufort Gyre

As variations in the Arctic density field are mainly driven by salinity and as our experiment protocol relies on continental freshwater fluxes sensitivity, we will investigate salinity budgets to assess the origin of the salinity contribution to regional sea level change. We use a set of offline diagnostics. The monthly salinity budget for any given grid cell can be written as follows:

$$\underbrace{\frac{\partial S}{\partial t}}_{H_{\text{total}}} = \underbrace{-\mathbf{u}\cdot\nabla S}_{H_{\text{advection}}} \underbrace{-\frac{\mathcal{F}}{\delta_s\,\rho_w}}_{H_{\text{forcing}}} + \underbrace{\text{LDF} + \text{ZDF} + \text{BBL} + \text{DMP} + \varepsilon}_{H_{\text{residual}}}, \tag{5}$$

where H_{total} is the total salinity change and is computed monthly using daily outputs (instead of instantaneous snapshots); $H_{\text{advection}}$ is the vertical and horizontal advection of salinity (i.e., salinity convergence and divergence) and is computed using the monthly averaged diagnostic of the products of velocity and salinity; H_{forcing} is the surface boundary condition which is calculated here using the monthly downward surface salt flux ($\mathcal{F}$) due to sea ice freezing and melting, the thickness of the surface layer (δ_s), and the density of freshwater (ρ_w); and H_{residual} is the nonresolved salinity changes which include lateral and vertical diffusion (LDF and ZDF, respectively), the bottom boundary layer (BBL) parametrization, the internal damping (DMP), and the approximations (ε) associated with using daily diagnostics for H_{total} instead of snapshots. H_{residual} is deduced by subtracting $H_{\text{advection}}$ and H_{forcing} from H_{total}. Given that H_{residual} is small compared to the other terms of the budget of the sensitivity experiments, we conclude that the missing diffusion terms and approximations are small and that our budget is precise enough to determine the major processes driving the salinity changes in the Beaufort Gyre. Then, for each term of the budgets, we compute the full-depth spatially weighted mean for a given enclosed volume.

To further analyze the advective term of a given freshwater source (Gr + Riv, GREENLAND, and RIVERS), the advective term was decomposed into three parts using the velocity and salinity fields changes generated by the given freshwater source. As the circulation of the Arctic Ocean is weakly sensitive to a given freshwater source (Figures S3–S5 in Supporting Information S1), we name the velocity and salinity field of exp2 the background circulation (i.e., the circulation unaffected by the time-varying Greenland discharge and river runoff). For instance, the decomposition of the advective term for GREENLAND is calculated as follows:

$$\begin{aligned} H^{\text{GR}}_{\text{advection}} &= H^{\text{exp1}}_{\text{advection}} - H^{\text{exp2}}_{\text{advection}}, \\ &= -\mathbf{u}_{\text{exp1}}\cdot\nabla S_{\text{exp1}} + \mathbf{u}_{\text{exp2}}\cdot\nabla S_{\text{exp2}}, \\ &= -\left(\mathbf{u}_{\text{exp2}} + \mathbf{u}_{\text{GR}}\right)\cdot\nabla\left(S_{\text{exp2}} + S_{\text{GR}}\right) + \mathbf{u}_{\text{exp2}}\cdot\nabla S_{\text{exp2}}, \\ &= -\mathbf{u}_{\text{bkgd}}\cdot\nabla S_{\text{GR}} - \mathbf{u}_{\text{GR}}\cdot\nabla S_{\text{bkgd}} - \mathbf{u}_{\text{GR}}\cdot\nabla S_{\text{GR}}, \end{aligned} \tag{6}$$

where $H^{GR}_{advection}$ is the salinity advection due to Greenland discharge fluctuations, $H^{exp1}_{advection}$ and $H^{exp2}_{advection}$ are the salinity advection terms in exp1 and exp2, respectively. $\mathbf{u}_{bkgd} = \mathbf{u}_{exp2}$ and $\mathbf{u}_{GR} = \mathbf{u}_{exp1} - \mathbf{u}_{exp2}$ are the background and GREENLAND velocity fields where $\mathbf{u}_{exp1}$ and $\mathbf{u}_{exp2}$ are the velocity of exp1 and exp2. $S_{bkgd} = S_{exp2}$ and $S_{GR} = S_{exp1} - S_{exp2}$ are the background and GREENLAND salinity fields where S_{exp1} and S_{exp2} are the salinity of exp1 and exp2. The first component is $-\mathbf{u}_{bkgd} \cdot \nabla S_{GR}$ and corresponds to the background advection of the salinity anomalies induced by changes in Greenland discharge. This term can be interpreted as the passive advection of salinity anomalies ("passive advection term" hereafter). The second component is $-\mathbf{u}_{GR} \cdot \nabla S_{bkgd}$ and corresponds to the advection by the anomalous velocity of the background salinity ("active advection term" hereafter). This term includes wave dynamics, for instance. The last component $-\mathbf{u}_{GR} \cdot \nabla S_{GR}$ corresponds to the advection of salinity anomalies by the anomalous velocity due to Greenland fluctuating discharge ("nonlinear advection term" hereafter).

Finally, we also define the time-cumulative salinity impact (G) of instantaneous change (H) as

$$G = \int_{t_0}^{t} H \, dt. \tag{7}$$

This formulation is applied to each component (i.e., total, advection, forcing, and residual) and each experiment (exp1, exp2, CLIM) and their differences (Gr + Riv, GREENLAND, and RIVERS). By definition, $G_{total} = S(t) - S(t_0)$, so that G reflects the salinity change at t since t_0 due to a particular component and a particular experiment.

3. Results

3.1. Model Assessment

We define a box in the BGR between 130–170°W and 70–81°N, and water depths greater than 300 m (black box in Figure 3 and Figure S1 in Supporting Information S1) as this definition has been largely used for investigations of freshwater and sea level changes (Proshutinsky et al., 2019; Fukumori et al., 2021; M.-L. Timmermans & Toole, 2023). We evaluate the reference run exp1 by comparing the SLA time series in the BGR box from exp1 and from the five altimetry products and ECCO V4r4.

To be able to compare the SLA from altimetry with the model, we remove from the radar altimetry data sets the GMSL (using the AVISO GMSL product without glacial isostatic adjustment) and their respective time means. As the altimetry-based products have different spatial and temporal coverage, we also compare exp1 with the global ocean-sea ice state estimate ECCO V4r4 (ECCO Consortium et al., 2021b). ECCO V4r4 is corrected using its own GMSL and time mean. Altimetry and ECCO V4r4 time series are shifted before plotting, using the model's time-averaged value over the overlap period of the data compared to exp1, to facilitate visual comparison in Figure 1.

Exp1 SLA (black curve in Figure 1) displays a standard deviation of 6.8 cm over the 1980–2018 period and a significant linear trend of 13.9 ± 3.2 mm yr^{-1} over 2005–2017. It decreases from 1980 to 1995 and increases afterward. The steepening of the black curve from 2012 attests an acceleration in the SLA increase of the Beaufort Gyre after 2012. This behavior is consistent with previously described Arctic circulation regime changes (Proshutinsky et al., 2015). Indeed, the SLA decrease over the 1980–1995 period can be associated with an oceanic cyclonic circulation regime and the following increase with an oceanic anticyclonic circulation regime still ongoing today (Proshutinsky et al., 2015). Also, the time series of the barotropic streamfunction in the BGR box of exp1 (Figure S3 in Supporting Information S1) shows a change in the circulation regime, shifting from negative to positive at the end of the 1990s. This transition from a cyclonic to an anticyclonic circulation might correspond to an atmospheric regime shift around 1990 (Kenigson & Timmermans, 2021).

On one hand, the altimetry products CCI DTU (from 1993 to 2017), Doglioni et al. (2021), Prandi et al. (2021), and CPOM (the last three data sets have the same time period 2011–2018) do not show any significant trend over their respective time coverage (red, green, pink, and blue curves in Figure 1, respectively). Their interannual variability is weaker than our model one with standard deviations of 3.4, 1.1, 1.1, and 1.9 cm, and they do not show significant correlation with exp1. On the other hand, the Armitage et al. (2016) product, which has one of the

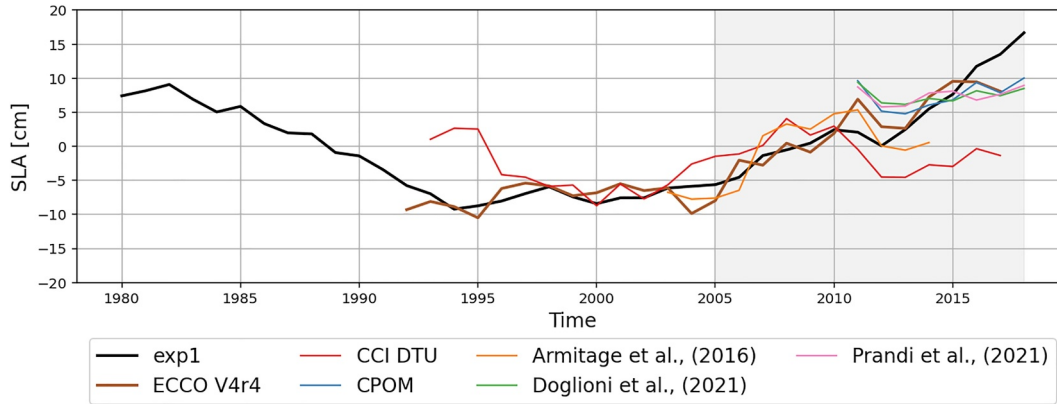

Figure 1. Sea level anomalies annual time series (1980–2018) in the Beaufort Gyre Region box of (black curve) the control run exp1 and of altimetry products: (red curve) CCI DTU (Rose et al., 2019), (blue curve) CPOM, (orange curve) Armitage et al. (2016), (green curve) Doglioni et al. (2021), (purple curve) Prandi et al. (2021), and (brown curve) the state estimate ECCO V4r4. Altimetry and ECCO V4r4 time series are shifted before plotting, using the model's time-averaged value over the overlap period of the data compared to exp1, to facilitate visual comparison. All time series are corrected from their respective global mean sea level and time mean. The period shaded in light gray corresponds to the period of interest 2005–2018.

longest time coverage, is closer to exp1 with a significant correlation coefficient of 0.82 and similar interannual variability (4.7 cm) and trend (9.3 ± 7.0 mm yr^{-1}, computed over 2003–2014) (orange curve in Figure 1).

There are two possible reasons why the Armitage et al. (2016) product is closer to the model than the other four altimetry products. Firstly, it stops in 2014 and therefore does not include the last few years, that are not well represented in the model, as shown by the Doglioni et al. (2021), Prandi et al. (2021), and CPOM products. Secondly, unlike CCI DTU, it does not use conventional altimetry data from the ERS-1 and ERS-2 satellites (covering the period 1993–2003) since their quality is questionable due to poor coverage and inability to discriminate between ice and leads resulting in the overestimation of SLA (Rose et al., 2019).

The Armitage et al. (2016) and CCI DTU product time series differ from each other probably due to the distinct processing methods applied to Envisat. Moreover, all the altimetry-based time series have been in good agreement since 2011, despite different processing methods, highlighting the improvement of data quality retrieved from SARAL/AltiKa and CryoSat-2 compared to previous satellites.

Exp1 SLA is in good agreement with ECCO V4r4 SLA (brown curve in Figure 1) with a significant correlation coefficient of 0.93. The ECCO V4r4 trend over 2005–2017 (12.7 ± 3.5 mm yr^{-1})—period of maximum overlap with our period of interest—is close to the model trend over the same period. It is worth pointing out that although ECCO V4r4 is a constrained ocean state estimate and exp1 a forced simulation, their regional SLA time series in the BGR box behave very similarly.

As exp1 is in agreement with satellite-based SLA from Armitage et al. (2016) and ECCO V4r4 in time and space (Figures S6 and S7 in Supporting Information S1), we feel confident to investigate the sea level change from our model in the BGR box.

3.2. Impact of Freshwater Flux Variability on Regional Sea Level Change and Its Components

3.2.1. Sea Level Change

In this section, we investigate the impact of fully varying continental freshwater fluxes from Greenland and rivers on sea level change in the BGR box. We find that all fully varying freshwater fluxes (Gr + Riv) lead to SLA interannual variability with a standard deviation of 3.7 mm and no long-term trend (black curve in Figure 2). Greenland discharge and river runoff (GREENLAND and RIVERS, respectively) show an opposite impact on SLA in the BGR (orange and blue curves in Figure 2, respectively). Over the 1980–2005 period, GREENLAND and RIVERS balance each other, and their combination (Gr + Riv) fluctuates around zero. Between 2006 and 2009, Gr + Riv SLA increased rapidly by 2.2 cm. This is due to a sharp increase in GREENLAND, not fully offset

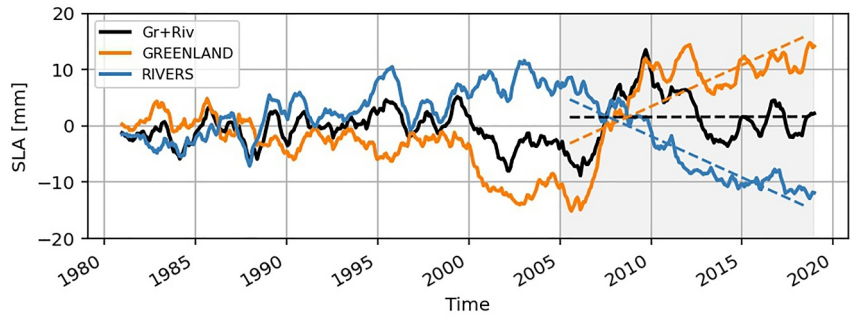

Figure 2. Monthly mean sea level anomalies time series in the Beaufort Gyre Region box with a 12-month running mean. The black curve represents exp1 minus CLIM (Gr + Riv), the orange curve exp1 minus exp2 (GREENLAND), and the blue curve exp2 minus CLIM (RIVERS). The dotted black, blue, and orange lines are the linear trends of their corresponding curves over 2005–2018. The gray shaded part highlights the period 2005–2018.

by RIVERS. Inversely, since 2010, RIVERS have impacted SLA at a higher rate than GREENLAND, re-balancing the Gr + Riv SLA curve. SLA trends over the 2005–2018 period for GREENLAND, RIVERS, and Gr + Riv are 1.47 ± 0.76 mm yr^{-1} (95% confidence interval), -1.47 ± 0.33 mm yr^{-1}, and 0.01 ± 0.72 mm yr^{-1}, respectively (orange, blue, and black dashed lines in Figure 2, respectively). These results indicate that, in the sensitivity differences, the variability in freshwater fluxes from both Greenland and rivers, has a significant impact on the BGR SLA over the period 2005–2018 when Greenland discharge and river runoff balance each other.

We now turn our attention to the spatial trend pattern of the SLA driven by fully varying freshwater fluxes in the Beaufort Gyre (Figures 3a–3c). The SLA trends in Gr + Riv, GREENLAND, and RIVERS explain roughly 10% of the SLA trends in exp1 in the BGR box (Figure S8 in Supporting Information S1). Over the period 2005–2018, relatively large trends are found in the Amerasian basin, particularly in the BGR box (maximum of 6.16 ± 2.07 mm yr^{-1} in GREENLAND and minimum of -6.94 ± 1.26 mm yr^{-1} in RIVERS), and weak trends, in the order of 1 mm year^{-1}, in the rest of the Arctic (shelf seas and Eurasian basin) (Figures 3a–3c). In the BGR box, the SLA trend pattern of Gr + Riv resembles the one of RIVERS with weaker trends on the eastern side and stronger trends on the western side (on the Chukchi Plateau), revealing that RIVERS dominate the signal (Figures 3a–3c). The proportion of RIVERS contribution to Gr + Riv SLA trends is 45% in the Arctic while it is 62% in the BGR box revealing a greater impact of RIVERS on sea level trend in this region. In the BGR box, the spatial pattern of the trends in RIVERS is a dipole and a positive monopole in GREENLAND (Figures 3b and 3c). RIVERS' dipole is positive on the Chukchi Plateau and negative in the Canada basin. It is worth noting that SLA significant trends are not only located in the BGR box but also extend out of the box in the Amerasian basin with a broad dipole pattern (Figures 3a–3c). We further decompose the sea level trend induced by fully varying freshwater fluxes into its steric and manometric components to better understand their contribution.

3.2.2. Sea Level Components Analysis

The steric trends over the 2005–2018 period are very similar to the SLA trends over the Arctic Ocean (Figures 3d–3f). The manometric trend maps are quite uniform and one order of magnitude lower than the steric ones (Figures 3g–3i). In the BGR box, the contribution of the steric trends to the SLA trends is 88% for Gr + Riv, 74% for GREENLAND, and 78% for RIVERS. This implies that the variability of the freshwater fluxes influences the SLA in the BGR box mostly via density changes, with the effects of addition/removal of mass being of a lower order. This is in accordance with Fukumori et al. (2021) who showed in ECCO V4r4 that manometric sea level is unrelated to the Beaufort Sea decadal change.

We further decomposed the full-depth steric sea level trends into their halosteric (Figures 3j–3l) and thermosteric (Figures 3m–3o) components for Gr + Riv, GREENLAND, and RIVERS respectively. For each of the freshwater sensitivities, the sum of the thermosteric and halosteric trends is roughly equal to the steric trends, showing that the nonlinearities are small. The halosteric maps are very similar to their corresponding SLA and steric maps over the entire Arctic Ocean. The halosteric trends in the BGR box explain 87%, 88%, and 90% of the steric trends for Gr + riv, GREENLAND and RIVERS, respectively. The thermosteric trends are quite spatially uniform and one

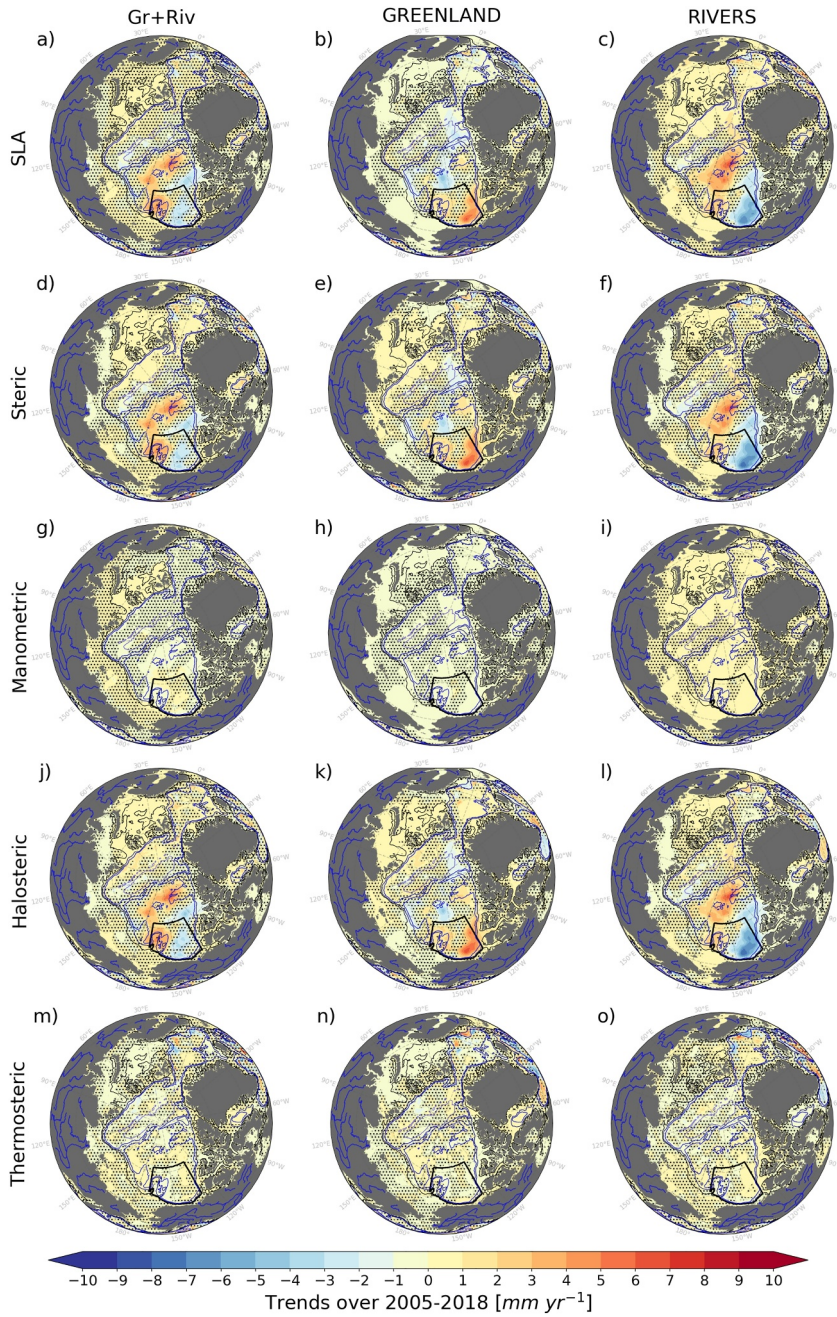

Figure 3. Sea level trend maps over 2005–2018 for Gr + Riv (left panels), GREENLAND (middle panels), and RIVERS (right panels). The rows from top to bottom show the sea level anomalies, the full-depth steric, manometric, halosteric, and thermosteric trends, respectively. The black thick contour line is the boundary of the Beaufort Gyre Region box. Bathymetry is contoured at 200, 1,000, 2,000, and 4,000 m. Gray stippling indicates the areas where the trends are statistically insignificant below the 90% confidence level using Wald Test with t-distribution.

order of magnitude lower than the halosteric trends for all sensitivity experiments in the BGR box. Therefore, freshwater flux variability affects sea level change in the BGR box mainly through changes in salinity.

To locate where the change occurs over depth, we investigate the vertical cumulative steric, thermosteric, and halosteric sea level trends (calculated following Equations 2–4) averaged in the BGR box for Gr + Riv, GREENLAND, and RIVERS respectively. Gr + Riv shows an overlap between the halosteric and steric curves (Figure 4a). Above 1,000 m, they form a peak with a maximum trend of 0.5 mm year^{-1} at 78-m depth, whereas the

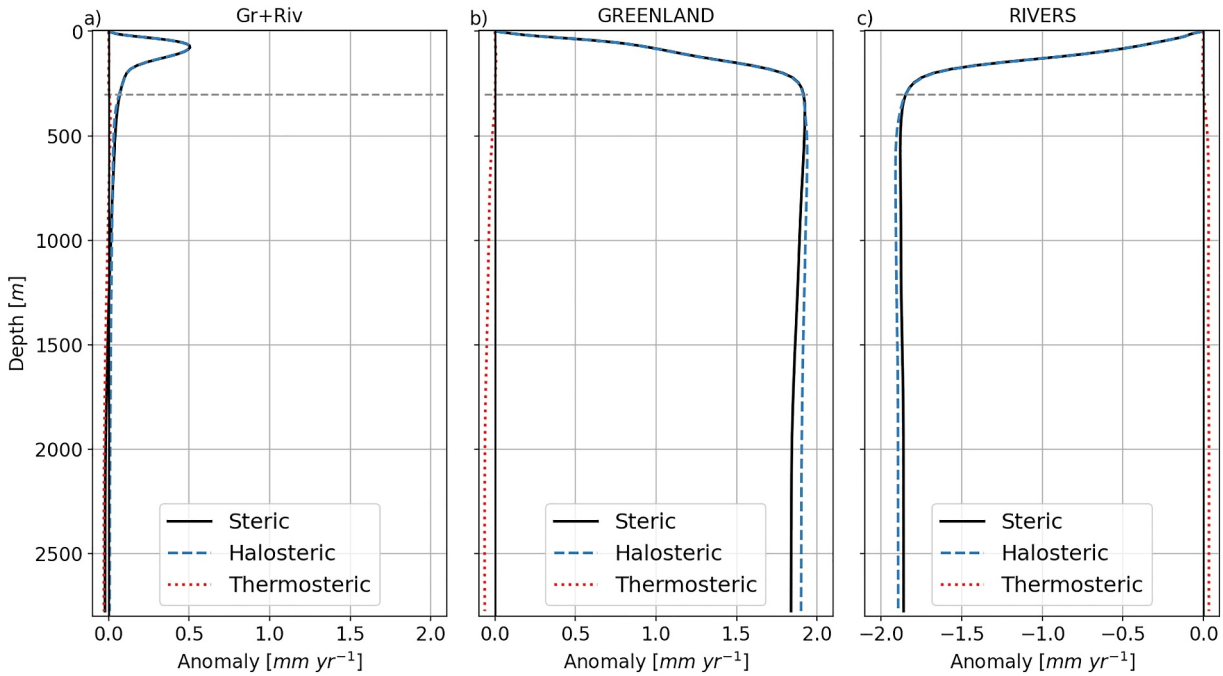

Figure 4. Depth-cumulative steric, halosteric, and thermosteric sea level trends over 2005–2018 from top to bottom for each model level (mm yr^{-1}) in the Beaufort Gyre Region box for (a) Gr + Riv, (b) GREENLAND, and (c) RIVERS. The horizontal dashed gray line represents 300-m depth.

thermosteric depth-trend remains close to zero. For Gr + Riv, the steric changes occur mainly in the upper 300 m and are dominated by the halosteric effect throughout the water column. When looking at GREENLAND and RIVERS, their depth-cumulative trend components mainly mirror each other with only slight differences (Figures 4b and 4c), responsible for the Gr + Riv variations. In GREENLAND and RIVERS, The depth-cumulative steric and halosteric trends are similar. From the surface to 300-m depth, they increase (decrease) steadily in GREENLAND (RIVERS). Below 300 m, the depth-cumulative halosteric trends stay constant while the depth-cumulative steric trends decrease (increase) slightly due to the depth-cumulative thermosteric trends in GREENLAND (RIVERS). The peak of the Gr + Riv depth-cumulative steric and halosteric trends results from the slight mismatch between GREENLAND and RIVERS: dominance of GREENLAND from 0 to 78 m and dominance of RIVERS from 78 to 300 m. It could seem surprising at first glance that GREENLAND has a greater impact on the upper ocean than RIVERS, given that rivers are forced from the surface to 10-m depth while water from Greenland can enter at greater depths. However, as it will be noted in Figure 6 and the discussion section, freshwater fluxes from rivers and Greenland act on the SLA in the BGR box through passive, active, and nonlinear advection.

This analysis confirms that the variability of Greenland and rivers fluxes act primarily on the salinity field leading to SLA changes mostly driven by halosteric effect. We highlight that, despite Greenland being far from the BGR, the variability of freshwater fluxes in GREENLAND contributes to a subsurface freshening in the BGR leading to an increase in SLA. In addition, our diagnostics indicate that the halosteric changes are mainly restricted to the upper 300 m of the ocean (in accordance with Fukumori et al. (2021)) while the thermosteric effect is minor, but deeper. The thermosteric effect in GREENLAND and RIVERS below 300-m deep probably corresponds to a warming and cooling, respectively, of the Atlantic water below the halocline (M.-L. Timmermans & Toole, 2023). In the case of Greenland, the salinity drop at the surface may strengthen the stratification in the halocline thus diminishing vertical mixing and hence vertical heat flux to the atmosphere from the Atlantic water layer. The reverse logic may explain the cooling of the Atlantic water layer in RIVERS.

3.3. Salinity Budget Analysis of the Beaufort Gyre Region Box

To assess the mechanisms of the salinity-driven sea level change, we perform salinity budgets. The monthly mean salinity budget in the BGR box helps us to assess whether changes in salinity are due to the advection term, an

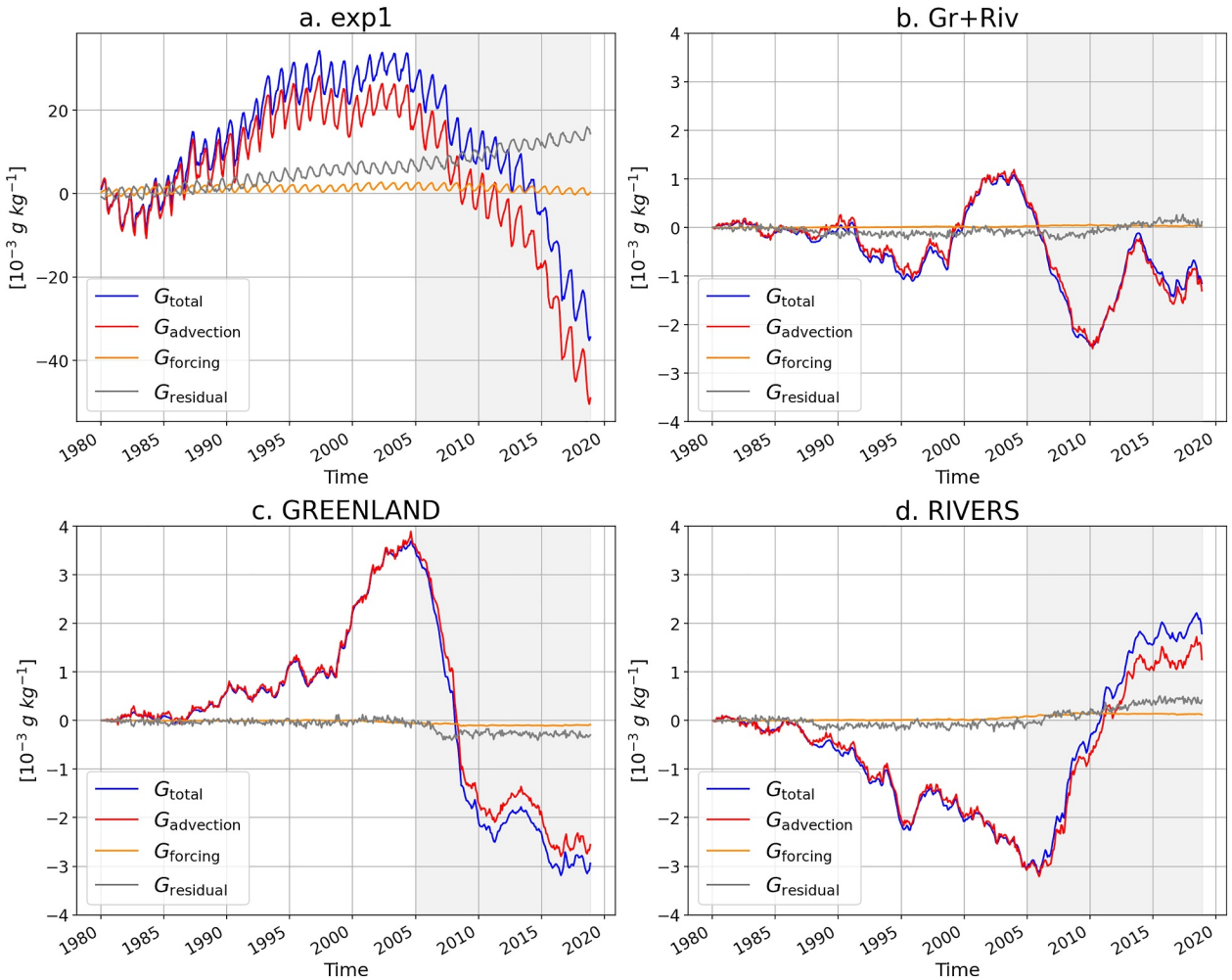

Figure 5. Time series of the time-cumulative monthly salinity of each full-depth budget term of the runs (a) exp1, (b) Gr + Riv, (c) GREENLAND, and (d) RIVERS in the Beaufort Gyre box for the period 1980–2018. The total salinity change is in blue, the advection term is in red, the forcing term corresponding to the salt flux from sea ice is in orange, and the residual term is in gray. The gray shaded part highlights the period 2005–2018, where trends are computed.

increase/decrease in local sea ice melt, or diffusion. The evolution of exp1 time-cumulative total salinity change (G_{total}) is in line with the exp1 SLA time series evolution (Figure 5a vs. Figure 1). G_{total} is highly anti-correlated with exp1 monthly SLA (correlation coefficient (CC) = −0.93), confirming that the halosteric component is behind most of the SLA changes. G_{total} is roughly constant from 1980 to 1984, then it rises up to 34.2×10^{-3} g kg^{-1} in 1995 and stays roughly stable until 2005 before decreasing from 2005 to 2018. G_{total} is decomposed into the advection term ($G_{\text{advection}}$), the forcing term corresponding to the salt flux with sea ice (G_{forcing}), and the residual term (G_{residual}) following Equation 5.

Exp1 G_{total} and $G_{\text{advection}}$ largely overlap at the start and gradually begin to diverge, demonstrating that the salinity evolution is dominated by advection, while G_{residual} increases linearly over the 1980–2018 period. G_{residual} cumulatively sums up over time a constant error associated with the approximation linked to the use of daily data (rather than snapshots) in the calculation of H_{total}. For Gr + Riv, GREENLAND, and RIVERS, G_{residual} is small and fluctuates around zero, showing that it cancels out for these sensitivity differences (Figures 5b–5d). This highlights that the approximation error is very similar between the experiments exp1, exp2, and CLIM. Therefore, we assume that this error does not impact our results and that the diffusion term remains small. The forcing term G_{forcing} fluctuates around zero throughout the simulation (Figures 5a–5d). G_{forcing} is thus negligible with respect to $G_{\text{advection}}$ that explains most of the total time-cumulative salinity change (Figures 5b–5d).

Gr + Riv's G_{total} shows a significant long-term negative trend over the period 1980–2018 of $-0.03 \pm 0.02 \times 10^{-3}$ g kg^{-1} yr^{-1} (Figure 5b). GREENLAND's G_{total} first increases from 1980 to 2004, reaching a maximum value of 3.7×10^{-3} g kg^{-1}, then decreases until 2018 (Figure 5c). RIVERS's G_{total} first decreases, reaching a minimum at the end of 2005 of -3.1×10^{-3} g kg^{-1}, then increases until 2018 (Figure 5d). Consequently, as with changes in SLA (Figure 2), the time-cumulative change in total salinity of the GREENLAND and RIVER sensitivity differences evolve in an opposite, almost compensatory manner, leading to the variations observed in Gr + Riv. The G_{total} curves of Gr + Riv, GREENLAND, and RIVERS are strongly anti-correlated to their corresponding SLA curves in Figure 2 ($CC = -0.73$, -0.96, and -0.93, respectively).

The time-cumulative full-depth salinity budget of exp1, Gr + Riv, GREENLAND, and RIVERS reveal that the salinity field evolution in the BGR box is dominated by advection. To better understand the change in advection in Gr + Riv, GREENLAND, and RIVERS, we further investigate the advection term by breaking it down into three terms following Equation 6.

For Gr + Riv, the passive advection term starts by decreasing until 1998 and then increases, while the active advection term starts by increasing until 1998 before decreasing (Figure 6a solid and dotted curves respectively). Thus, these two advection terms behave very similarly with opposite signs, counterbalancing each other quite well (as expected for geostrophic flow–i.e., the non-Doppler effect, Held, 1983; Killworth et al., 1997; Liu, 1999; Rossby, 1939). The nonlinear term follows closely the $G_{\text{advection}}$ evolution and displays weak values throughout most of the simulation (Figure 6a, dashed curve) (this is also expected in a geostrophic flow where gradients of density anomalies are orthogonal to the flow anomaly).

For GREENLAND (Figure 6b), the nonlinear term and the active advection term behave quite similarly with opposite signs, largely compensating each other. The passive advection term is close to the $G_{\text{advection}}$ curve in magnitude and follows a similar evolution, first increasing until 2005 and then decreasing. Over 2005–2018, the decrease in $G_{\text{advection}}$ (Figure 6b, red curve) is due to the passive advection and large compensations of the nonlinear and active terms highlighting the complex nonlinear dynamics of the Arctic Ocean in GREENLAND.

For RIVERS (Figure 6c), the three advection components evolve very differently. Over 2005–2018, the passive advection increases rapidly, while the other two terms decrease, leaving a weak increase of $G_{\text{advection}}$. Hence, the evolution over 2005–2018 of the $G_{\text{advection}}$ term in GREENLAND and RIVERS is due to the passive advection being compensated by the other two.

We have shown in this section that the variations of SLA in the BGR box in all sensitivity differences are primarily due to the advection of salinity. Furthermore, the three components of the salinity advection term are equally important and large compensations occur between them.

4. Discussion

The present study reports the potential impact of Greenland ice sheet melting and river runoff variability on sea level trends in the Beaufort Gyre.

For Greenland impact, we find large trend values over 2005–2018 in the Beaufort Gyre of up to 6.16 ± 2.07 mm yr^{-1}. Several studies also investigated the oceanic response to Greenland melting in forced ocean models using a sensitivity approach. Stammer (2008) found a sea level increase in the Atlantic Ocean associated with a permanent positive surface freshwater runoff anomaly off the lower half of Greenland in the MITgcm over a 50-year simulation. Marsh et al. (2010) evaluated the short-term impact (8 years) of a sudden and sustained climatogical increase of Greenland surface meltwater with realistic geographical distribution in NEMO. They found that it impacts the Arctic Ocean's salinity off the north coast of Greenland via a northward advection of freshwater anomalies fluxed onto the northeast Greenland shelf by a narrow coastal current. We also find in our simulations a northward narrow coastal current off the Northeast Greenland shelf (Figure S9 in Supporting Information S1). However, the northward salinity transport by this current is very similar between simulations and thus might not be sufficient to explain the differences in the BGR between our simulations. Dukhovskoy et al. (2019) forced Greenland freshwater flux realistically using the products of Bamber et al. (2012, 2018) between the surface and 6 m depth and released passive tracers to track the anomalous freshwater. They found that 44% of the volume of the Greenland freshwater anomaly is retained in the subpolar North Atlantic by the end of the 24-year simulation (1993–2016) and is mixed down to several hundred meters without entering in the Arctic Ocean. Despite different forcings of Greenland melting, these studies show little or no impact on the Arctic Ocean

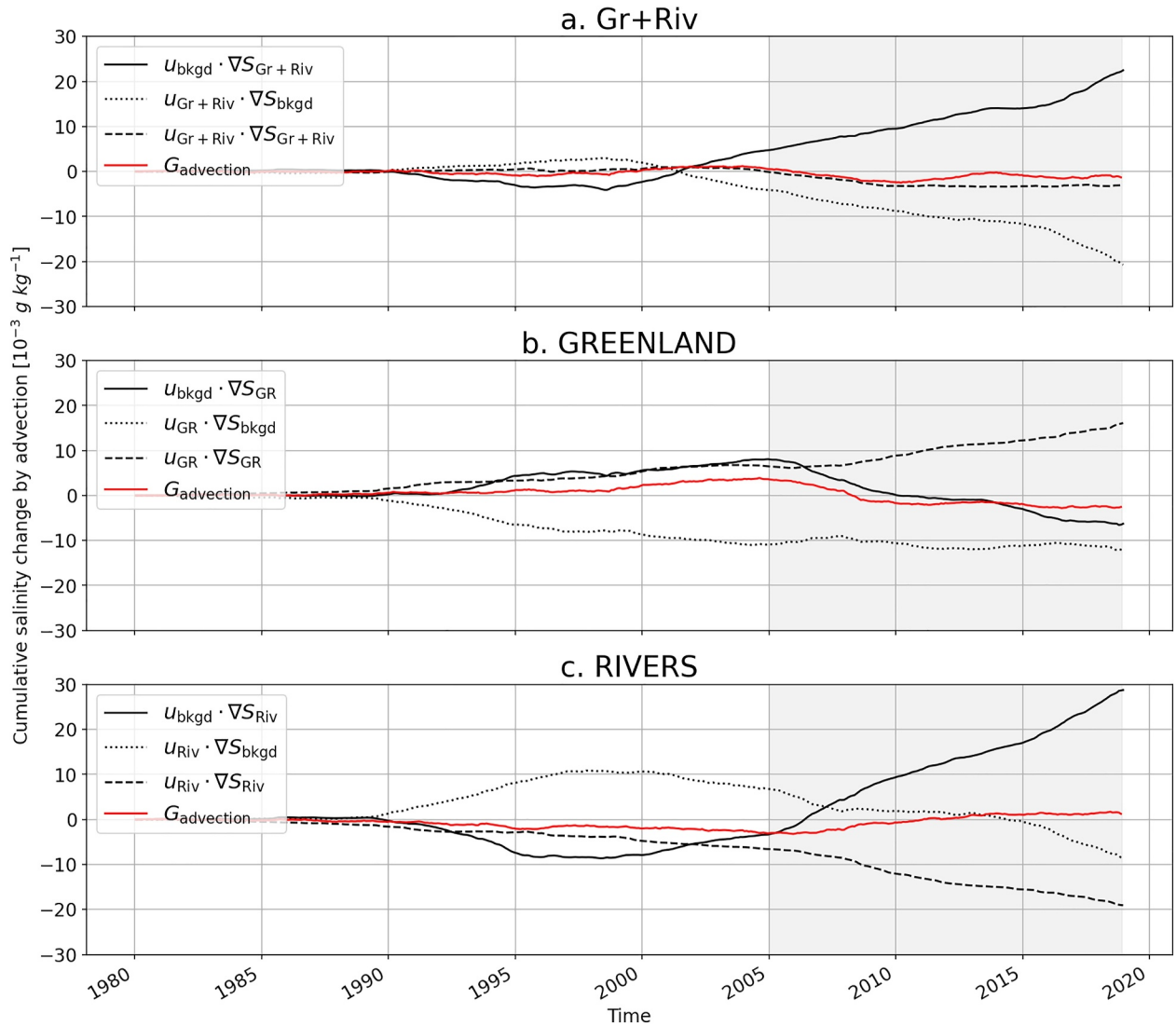

Figure 6. Time series of the decomposition of the time-cumulative full-depth salinity advection term of (a) Gr + Riv (exp1 − CLIM), (b) GREENLAND (exp1 − exp2), and (c) RIVERS (exp2 − CLIM). The components of the advective term are: the advection of the salinity anomalies by the background circulation ("passive advection term", solid curve), the advection of the background salinity by the anomalous velocity ("active advection term", dotted curve), and the nonlinear–the advection of the salinity anomalies by the anomalous velocity–advection (dashed curve). The $G_{advection}$ term of Figure 5 for each sensitivity difference is also plotted in red. The gray shaded part highlights the period 2005–2018 where trends are computed.

overall but rather on the Atlantic Ocean which was their prime interest in the first place. Our result is probably due to the new method used to perform Greenland forcing in our simulations: a fully time-varying realistic liquid and solid discharge distributed around Greenland in the nearest gridcell to glacier terminations and varying with depth (Figure S2 in Supporting Information S1). Injecting the freshwater at depth in our simulations probably have an impact on its mixing and on how it affects the regional salinity field of the Atlantic Ocean. This idea is supported by the difference in salinity transport between simulations across a section from Greenland to Svalbard (Figure S9 in Supporting Information S1).

Furthermore, we also consider the impact of the full variability of river runoff on sea level in the BGR. This has not been done before as previous studies either focused on its impact on other features of the Arctic ocean (stratification, circulation, sea ice, and freshwater content, Hall et al., 2023; Lambert et al., 2019; Nummelin et al., 2016), or focused on the sea level but using climatological forcing for rivers in their model (Jahn et al., 2012; Piecuch & Wadehra, 2020; Proshutinsky et al., 2019). Chandanpurkar et al. (2022) is the only study to our knowledge that quantifies the impacts of nonseasonal river discharge (from the daily discharge JRA55-do data set

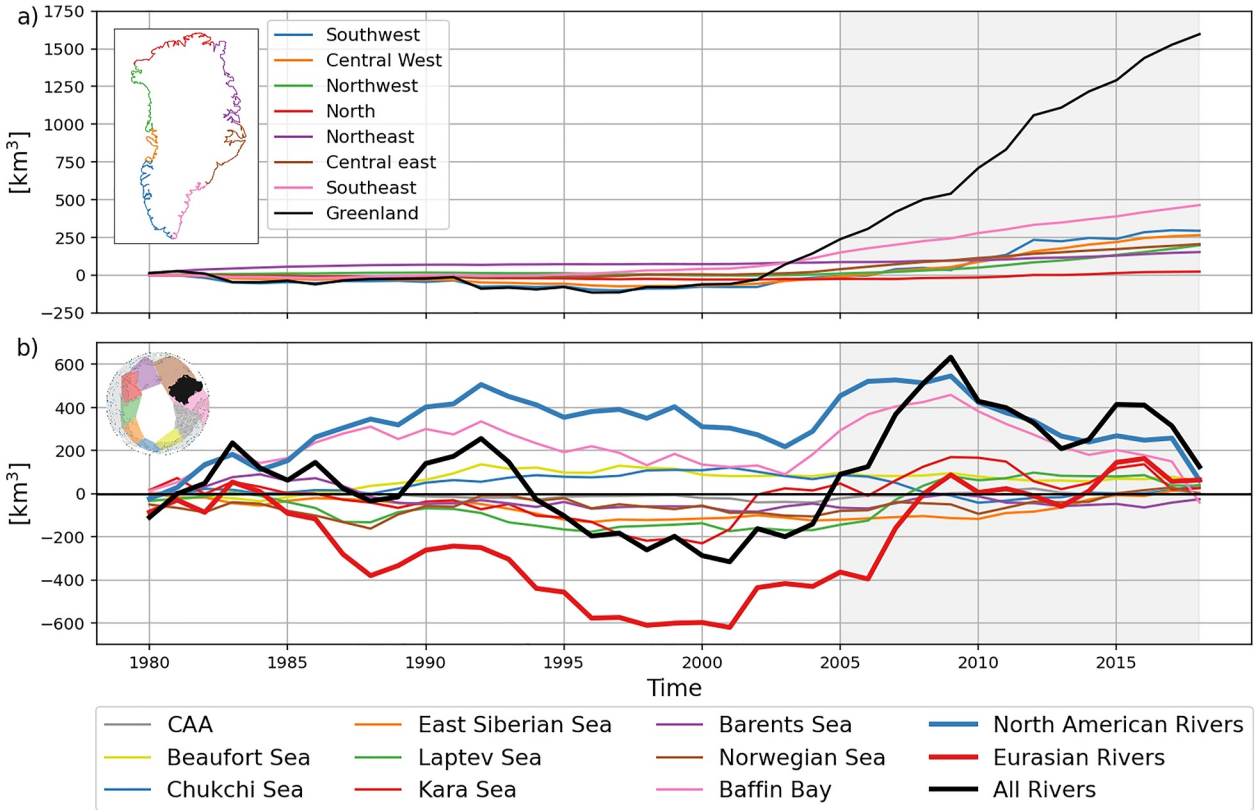

Figure 7. Time-cumulative annual time series of freshwater fluxes forcing in GREENLAND (a) and RIVERS (b) in km^3. North American rivers correspond to masks "Chukchi Sea," "Baffin Bay," "Beaufort Sea," and "CAA." Eurasian rivers correspond to masks "East Siberian Sea," "Laptev Sea," "Kara Sea," "Barents Sea," and "Norwegian Sea."

of Suzuki et al. (2018)) on sea level in a global forced model (MITgcm). However, their analysis is restricted to ocean regions in direct proximity with the 10 major river mouths. Hordoir et al. (2022) shows that trends in river runoff can change the Arctic coastal dynamics which can in turn locally decrease but also increase salinity.

One of the main results of our study is the opposite impact of GREENLAND and RIVERS and their partial compensation on SLA in the BGR box. Since only the freshwater forcing varies between simulations, we now discuss the forcing of the freshwater fluxes. For GREENLAND, the time-cumulative annual time series of freshwater discharge (black curve in Figure 7a) shows that GREENLAND slightly increased ocean salinity before 2003, but strongly freshened it after 2003. This is due to the fact that Greenland climatology was computed over the period 1950–1972 and not 1980–2018. The temporal evolution of the time-cumulative discharge of Greenland in GREENLAND is consistent with the evolution of the SLA and the time-cumulative salinity in the BGR (orange curve in Figures 2 and 5c). It suggests that salinity field differences in GREENLAND induced by Greenland discharge variability are potentially reflected in the BGR. The whole ice sheet has been losing mass every year since 2000 (Figure S10a in Supporting Information S1). Greenland's discharge acceleration in GREENLAND over the 2000–2018 period is 0.13 mSv year^{-1} with all regions displaying an acceleration. The strongest discharge acceleration over 2000–2018 is found in the northwest region (0.044 mSv year^{-1}) followed by the central west region (0.023 mSv year^{-1}). The regions contributing the most in terms of freshwater volume discharged are the southeast, southwest, and central west regions, but further studies are needed to evaluate whether some regions of Greenland contribute more than others to the SLA rise in the BGR.

Although RIVERS represent the impact of global river runoff variability, we assume that only the rivers contributing to the Arctic Ocean freshwater budget can impact the regional SLA in the BGR. Therefore, we perform the freshwater forcing analysis only in the pan-Arctic region using masks shown in the subpanel of Figure 7b. Two spatial groups of river runoff could be distinguished based on the time-cumulative annual time series of river runoff in RIVERS (Figure 7b). First, North American rivers (masks "Chukchi Sea," "Baffin Bay",

"Beaufort Sea," and "CAA") show a similar behavior individually and together show a time-cumulative positive flux over 1980–2018 that increases over 1980–2005 and decreases over 2006–2018 (thick blue curve in Figure 7b). This broad evolution is similar with the evolution of the SLA time series and the time-cumulative salinity in the BGR box in RIVERS (blue curve in Figures 2 and 5d). Second, Eurasian rivers (masks "East Siberian Sea," "Laptev Sea", "Kara Sea," "Barents Sea," and "Norwegian Sea") also show a similar behavior individually and together show a time-cumulative negative flux over 1980–2008 that increases over 1980–2001 and decreases over 2002–2008 before fluctuating around zero over 2009–2018 (thick red curve in Figure 7b). Thus, it suggests that, over 2005–2018, North American Rivers may have impacted the SLA in the BGR, while Eurasian Rivers may have not. This is in accordance with Proshutinsky et al. (2009) who showed that a very small amount of the freshwater from Siberian rivers was reaching the BGR between 2003 and 2014. Further investigations are needed to fully understand which rivers contribute to the SLA change in the BGR.

In GREENLAND, the time-cumulative discharge trend of Greenland has been positive since 2000, while in RIVERS, the time-cumulative runoff trend of North American Rivers has been negative since 2005 (black curve in Figure 7a and thick blue curve in Figure 7b). This opposite temporal evolution from 2005 in the time-cumulative forcing of GREENLAND and RIVERS is consistent with the opposite sea level response in the BGR in GREENLAND and RIVERS and could possibly explain it. It is worth noticing that the interannual variability introduced in the freshwater fluxes in GREENLAND and RIVERS is not of the same nature. It consists mostly in trends for GREENLAND and in fluctuations (not trends) for RIVERS (Figure S10 in Supporting Information S1). Thus, our study emphasizes the importance of including the fully varying freshwater fluxes as a whole to investigate regional sea level trends in the Arctic Ocean.

Changes in Greenland time-cumulative discharge are much larger than changes in North American rivers time-cumulative runoff, yet they produce comparable SLA changes in the BGR box. This suggests that BGR sea level is more sensitive to North American river runoff than to Greenland discharge, probably because of its geographic proximity. For instance, under anticyclonic circulation, floats released at the Mackenzie River mouth reach the BGR in around 1 year through Ekman transport convergence (Proshutinsky et al., 2009). On the other hand, Greenland's discharge is located further away and potentially impacts the SLA in the BGR through a range of different mechanisms.

For GREENLAND and RIVERS sensitivity differences, maps of time-lagged correlations between the full column mean salinity changes at each grid point and the time series of SLA in the BGR box have been computed (Figure S11 in Supporting Information S1). These maps tracked the correlations in time and space. The correlations do not indicate a specific area of high correlation. In addition, the strong anti-correlation within the BGR box faded out after around 5 years without reaching prescribed sources of freshwater (i.e., Greenland or rivers). We concluded that tracking backward in time the location of salinity changes from the BGR box to their origin was not possible through correlation. This is consistent with the fact that salinity has an active role (active and nonlinear advection terms) in changing the salinity in the BGR box and is not simply passively advected (Figure 6). Thus, as expected for an active tracer, such as salinity, it is likely not a direct passive impact of the water released by Greenland (or rivers) that modifies sea level in the BGR, but rather a complex response involving both changes in circulation and salinity. Greenland discharge may impact water column stability, the North Atlantic subpolar gyre system, and the Atlantic Meridional Overturning Circulation which in turn may affect the patterns of sea-level rise (Lorbacher et al., 2010; Proshutinsky et al., 2015; Stammer, 2008; Swingedouw et al., 2013). River runoff variability can modify coastal dynamics which would lead to salinity changes offshore (Hordoir et al., 2022). It would be interesting to further quantify the role of the passive versus active advection using the methodology of Stephenson and Sévellec (2021) applied to salinity. In addition, further investigations are needed to determine whether our results are reproducible with other models or can be identified in observations.

The sea level response to the freshwater variability is mainly halosteric in accordance with the literature (Carret et al., 2017; Fukumori et al., 2021; Lyu et al., 2022; Raj et al., 2020). Halosteric changes in the BGR box are largely caused by salinity advection (Figure 5). In GREENLAND and RIVERS, the salinity advection term is the result of large compensations between the passive advection on one hand, and the active and nonlinear advection on the other hand (Figure 6). In addition, we find that it is restricted to the upper 300 m (Figure 4). Similarly, Fukumori et al. (2021) found in ECCO V4r4 that the interannual sea level change in the BGR is mostly associated with horizontal convergence modifying its freshwater content nearly uniformly down to 200-m depth. This may

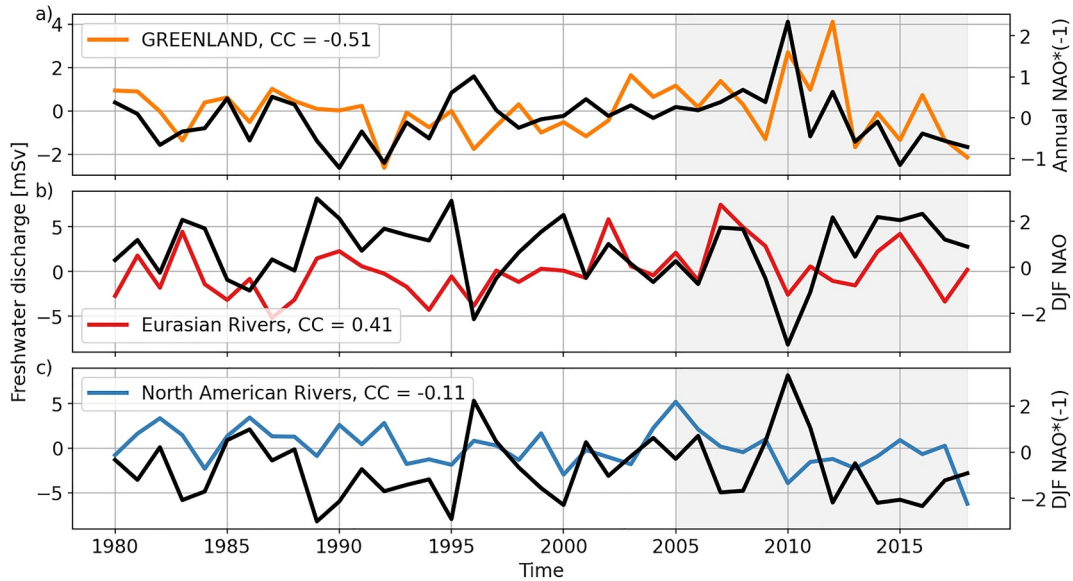

Figure 8. (a) Detrended annual freshwater discharge of Greenland in GREENLAND using a second order polynomial fit (orange curve) against the annual NAO index (black curve). (b) Eurasian and (c) North American rivers annual freshwater flux in RIVERS (red and blue curves respectively) against the wintertime NAO index (black curve). The Pearson correlation coefficient (CC) is indicated in the captions of (a–c). To facilitate visual comparison, the NAO index has been multiplied by −1 in (a and c).

result from the fact that the Arctic Ocean is strongly stratified with very low vertical turbulent mixing and diffusion leading to low vertical fluxes of freshwater (Solomon et al., 2021). However, Fukumori et al. (2021) also found that, at decadal time scales, the effect of sea ice meltwater accumulates and thus also contributes to sea level rise in the BGR.

Atmospheric circulation patterns influence the Arctic Ocean's freshwater input (Bring et al., 2016; Carmack et al., 2016; Solomon et al., 2021; Vihma et al., 2016). Meteoric water is one of the main sources of the Arctic Ocean's freshwater and includes river runoff (mainly from precipitation over land) and continental melt water including those from Greenland. In turn, precipitation over land is largely driven by atmospheric moisture transport (Solomon et al., 2021). Enhanced poleward atmospheric moisture transport across 60°N was found over 1979–2018 using ERA5 reanalysis (Nygård et al., 2020) and over 1950–2015 from NCEP-NCAR reanalysis (Villamil-Otero et al., 2018; Zhang et al., 2013). The enhanced poleward atmospheric moisture transport in turn is driven by the large-scale atmospheric circulation, namely the Arctic Oscillation (AO) (Kryzhov & Gorelits, 2015) and North Atlantic Oscillation (NAO). Furthermore, the figures AIV.1d and e of the IPCC (2021) show that a teleconnection exists between the boreal winter (DJF) NAO and the near-surface temperature and precipitation over land in the Arctic region. It means that the NAO potentially influences river runoff and Greenland discharge by affecting surface air temperature and precipitation over land. The NAO and AO patterns overlap and they are highly correlated in time (Dickson et al., 2000; Moritz et al., 2002). Here, we focus on the NAO index (Jones et al., 1997) and compare it with our freshwater flux forcing in the sensitivity experiments to test the influence of the NAO on freshwater flux variability.

We detrend the annual freshwater discharge of Greenland in GREENLAND (orange curve in Figure 8a) prior comparison with the annual NAO index, as we focus here on the interannual variability rather than on long-term trend. The acceleration of Greenland discharge since the 1990s can be attributed to rising air temperatures, changes in precipitation (Hanna et al., 2013), and to the warming of the subpolar North Atlantic ocean itself due to atmospheric changes (Straneo & Heimbach, 2013). We compare it to the annual NAO index (and not wintertime NAO) as we have found that the wintertime NAO index is significantly correlated to GREENLAND annual freshwater discharge with 1 year lag (not shown). The detrended annual Greenland discharge in GREENLAND and the annual NAO index time series anti-correlate well over the simulation period (CC = −0.51, significant) (Figure 8a). The annual freshwater flux of Eurasian rivers is significantly correlated with the DJF NAO index (CC = 0.41, Figure 8b), while that of North American rivers is not significantly correlated (CC = −0.11,

Figure 8c). These correlations suggest that Eurasian runoff in RIVERS and Greenland discharge in GREENLAND are influenced by the NAO whereas North American river runoff is not. These results are in accordance with the Fig. AIV.1d of the IPCC (2021) showing a regression map of the blended sea surface temperature and surface air temperature over land for 1959–2019 with the DJF NAO. Fig. AIV.1d of the IPCC (2021) shows significant strong positive (negative) correlation over Northern Europe and the Russian sector (Greenland Ice Sheet), and weakly negative to not significant correlations over the North American continent. The significant correlations between the freshwater flux variability in the sensitivity experiments and the NAO index support the hypothesis that the freshwater flux variability could be partly driven by the NAO. However, further studies are needed as the NAO also influences the pathways of river runoff which can also modulate the amount of freshwater reaching the BGR (Morison et al., 2021).

It is worth mentioning that our study presents some limitations coming from the model setup of the freshwater forcing. First, regarding river runoff, the ISBA-CTRIP model displays two weaknesses in boreal regions: a general underestimation due to high soil moisture content over high latitudes, and a too early springtime peak over all Arctic basins due to simulated early snowmelt (Decharme et al., 2019). Thus, future investigations should rely on a more realistic freshwater forcing set to better assess sea level change from river runoff in the Arctic Ocean. Secondly, accounting for the solid discharge from Greenland in the form of icebergs raised the challenge of prescribing a calving rate. This rate is used to take into account the melting of icebergs in fjords before reaching the first model sea point. The proportion of icebergs that melt in the fjords is very uncertain. Moyer et al. (2019) mentioned that for Sermilik Fjord 90% of the iceberg volume is lost in the fjord, but large uncertainties remain (Benn et al., 2017; Moon et al., 2018; Straneo et al., 2013), hence our choice of 50% of iceberg melt in the fjord. Furthermore, this study is based on the assumption that the model response to river runoff and Greenland discharge is additive. The GREENLAND sensitivity experiment (exp1 − exp2) is not an independent experiment in which Greenland discharge is fully varying and river runoff is a repeated seasonal cycle, but it has been assumed as such. GREENLAND also includes the non-linearities of the exp1 experiment, which we have assumed to be small. Finally, our model resolution limits the representation of mesoscale eddies in the Arctic Ocean. Yet, mesoscale eddies are essential for the Beaufort Gyre dynamics and have been shown to constrain its variation in freshwater content on interannual time scales (Hochet et al., 2024; Manucharyan & Spall, 2016; Manucharyan et al., 2016). Therefore, it would be of interest for future studies to use higher resolution numerical models that resolve eddies in the Arctic region.

5. Conclusions

The sea level trend sensitivity to fully varying freshwater flux from Greenland and rivers over the 2005–2018 period in the Beaufort Gyre region is studied in a forced global ocean model including sea-ice and iceberg. We find that Greenland's discharge and river runoff temporal changes produce an opposite impact on sea level trends in the BGR box, the former driving an increase while the latter a decrease. The combined impact of Greenland and rivers variability leads to barely any sea level trend in the BGR box. Greenland and rivers variability drive sea level changes in the BGR primarily via salinity variations in the upper 300 m, themselves mainly caused by salinity advection involving complex compensations between passive, active, and nonlinear advection. The SLA in the BGR in GREENLAND and RIVERS is impacted through changes in salinity and velocity and their interactions.

This study sheds light on the importance of considering the variability of both Greenland discharge and river runoff simultaneously to better understand regional sea level trends in the BGR. We find that both freshwater sources involve the same processes in the ocean and may counterbalance each other in the BGR. This topic is of great importance as Greenland will continue to lose mass and therefore it may no longer be counterbalanced by rivers in the BGR.

More investigations are needed to fully understand both Greenland discharge and river runoff contributions to regional sea level trends and variability. To study the robustness of our results, further sensitivity studies are needed with other models. Furthermore, specific studies to assess the impact of the injection of Greenland freshwater fluxes over different depths are needed as its advection relies on the depth-dependant circulation along Greenland's coast.

Data Availability Statement

To reproduce the simulations, the model code (NEMO 4.0.6) can be downloaded at http://forge.ipsl.jussieu.fr/nemo.wiki/Users.; the JRA-55 reanalysis is available at (Japan Meteorological Agency, Japan, 2013); and a thorough description of the configuration of the model is available at (Molines & Leroux, 2024). The Jupyter notebooks used to produce our analyses can be found at (Tajouri, 2024). The continental freshwater fluxes used in the simulations are taken from Mouginot et al. (2019) for Greenland ice sheet, Decharme et al. (2019) for rivers, and Rignot et al. (2013) for Antarctica. Arctic dynamic topography data were provided by the Centre for Polar Observation and Modelling (CPOM), University College London (www.cpom.ucl.ac.uk/dynamic_topography) and Armitage et al. (2016, 2017). The CCI DTU data set is provided by Rose et al. (2019). The data set of Doglioni et al. (2021) can be downloaded at Pangaea. The data set of Prandi et al. (2021) was processed by SSALTO/DUACS (Prandi & Veillard, 2020) and distributed by AVISO+ with support from CNES. ECCO Central Estimate (Version 4 Release 4) was retrieved from https://ecco-group.org/products.htm. and its GMSL time series from (ECCO Consortium et al., 2021a). The AVISO GMSL is available at (AVISO+, 2024). The NAO index was provided by Hurrell et al., (2019).

Acknowledgments
This work is a contribution to the IMHOTEP project which is supported by the Centre National d'Etudes Spatiales (CNES) through the Ocean Surface Topography Science Team (OSTST). ST is supported by a UBO-CNES PhD fellowship. WL and FS are supported by the EERIE project (Grant Agreement No 101081383) funded by the European Union. FS is supported by the ARVOR project funded through the French CNRS/INSU/LEFE program and by the CLIMArcTIC project funded by the "PPR Océan et Climat–France 2030." The simulations and computations were performed at Jean-Zay supercomputer operated by the CNRS Institut du Développement et des Ressources en Informatique Scientifique (IDRIS). Storage, data access, computational resources, visualization, web-services, consultation, support services. We thank Chris Piecuch, Mike Wood and two other anonymous reviewers for their comments and suggestions, which helped us to improve the manuscript. We dedicate this article to our colleague Jérémie Mouginot who passed away over the course of this study.

References

Andersen, O. B., & Piccioni, G. (2016). Recent Arctic Sea Level variations from satellites. *Frontiers in Marine Science*, *3*. https://doi.org/10.3389/fmars.2016.00076

Armitage, T. W. K., Bacon, S., Ridout, A. L., Petty, A. A., Wolbach, S., & Tsamados, M. (2017). Arctic Ocean surface geostrophic circulation 2003–2014. *The Cryosphere*, *11*(4), 1767–1780. https://doi.org/10.5194/tc-11-1767-2017

Armitage, T. W. K., Bacon, S., Ridout, A. L., Thomas, S. F., Aksenov, Y., & Wingham, D. J. (2016). Arctic sea surface height variability and change from satellite radar altimetry and GRACE, 2003–2014: Arctic SSH variability. *Journal of Geophysical Research: Oceans*, *121*(6), 4303–4322. https://doi.org/10.1002/2015JC011579

AVISO+. (2024). Mean sea level time series [Dataset]. *EU Copernicus Marine Service/CNES/LEGOS/CLS*. Retrieved from https://aviso.altimetry.fr/msl

Bamber, J., Van Den Broeke, M., Ettema, J., Lenaerts, J., & Rignot, E. (2012). Recent large increases in freshwater fluxes from Greenland into the North Atlantic: Freshwater into the North Atlantic. *Geophysical Research Letters*, *39*(19), L19501. https://doi.org/10.1029/2012GL052552

Bamber, J. L., Westaway, R. M., Marzeion, B., & Wouters, B. (2018). A new synthesis of annual land ice mass trends 1992 to 2016 [Dataset]. *PANGAEA*. (Supplement to: Bamber, JL et al. (2018): The land ice contribution to sea level during the satellite era. Environmental Research Letters, 13(6), 063008.). https://doi.org/10.1594/PANGAEA.890030

Barnier, B., Madec, G., Penduff, T., Molines, J.-M., Treguier, A.-M., Le Sommer, J., et al. (2006). Impact of partial steps and momentum advection schemes in a global ocean circulation model at eddy-permitting resolution. *Ocean Dynamics*, *56*(5), 543–567. https://doi.org/10.1007/s10236-006-0082-1

Benn, D. I., Cowton, T., Todd, J., & Luckman, A. (2017). Glacier calving in Greenland. *Current Climate Change Reports*, *3*(4), 282–290. https://doi.org/10.1007/s40641-017-0070-1

Bring, A., Fedorova, I., Dibike, Y., Hinzman, L., Mård, J., Mernild, S. H., et al. (2016). Arctic terrestrial hydrology: A synthesis of processes, regional effects, and research challenges. *Journal of Geophysical Research: Biogeosciences*, *121*(3), 621–649. https://doi.org/10.1002/2015JG003131

Campin, J.-M., Marshall, J., & Ferreira, D. (2008). Sea ice-ocean coupling using a rescaled vertical coordinate zlowast. *Ocean Modelling*, *24*(1), 1–14. https://doi.org/10.1016/j.ocemod.2008.05.005

Carmack, E. C., Yamamoto-Kawai, M., Haine, T. W. N., Bacon, S., Bluhm, B. A., Lique, C., et al. (2016). Freshwater and its role in the arctic marine system: Sources, disposition, storage, export, and physical and biogeochemical consequences in the Arctic and global oceans. *Journal of Geophysical Research: Biogeosciences*, *121*(3), 675–717. https://doi.org/10.1002/2015JG003140

Carret, A., Johannessen, J. A., Andersen, O. B., Ablain, M., Prandi, P., Blazquez, A., & Cazenave, A. (2017). Arctic Sea level during the satellite altimetry era. *Surveys in Geophysics*, *38*(1), 251–275. https://doi.org/10.1007/s10712-016-9390-2

Chandanpurkar, H. A., Lee, T., Wang, X., Zhang, H., Fournier, S., Fenty, I., et al. (2022). Influence of Nonseasonal River Discharge on Sea Surface salinity and height. *Journal of Advances in Modeling Earth Systems*, *14*(2), e2021MS002715. https://doi.org/10.1029/2021MS002715

Chen, X., Zhang, X., Church, J. A., Watson, C. S., King, M. A., Monselesan, D., et al. (2017). The increasing rate of global mean sea-level rise during 1993–2014. *Nature Climate Change*, *7*(7), 492–495. https://doi.org/10.1038/nclimate3325

Cheng, Y., Andersen, O., & Knudsen, P. (2015). An improved 20-year Arctic Ocean Altimetric sea level data record. *Marine Geodesy*, *38*(2), 146–162. https://doi.org/10.1080/01490419.2014.954087

Decharme, B., Delire, C., Minvielle, M., Colin, J., Vergnes, J.-P., Alias, A., et al. (2019). Recent changes in the ISBA-CTRIP land surface system for use in the CNRM-CM6 climate model and in global off-line hydrological applications. *Journal of Advances in Modeling Earth Systems*, *11*(5), 1207–1252. https://doi.org/10.1029/2018MS001545

Dickson, R. R., Osborn, T. J., Hurrell, J. W., Meincke, J., Blindheim, J., Adlandsvik, B., et al. (2000). The arctic ocean response to the North Atlantic oscillation. *Journal of Climate*, *13*(15), 2671–2696. https://doi.org/10.1175/1520-0442(2000)013⟨2671:TAORTT⟩2.0.CO;2

Doglioni, F., Ricker, R., Rabe, B., Barth, A., Troupin, C., & Kanzow, T. (2021). Pan-Arctic monthly maps of sea surface height anomaly and geostrophic velocity from the satellite altimetry Cryosat-2 mission [Dataset]. *PANGAEA*, 2011–2020. https://doi.org/10.1594/PANGAEA.931869

Dukhovskoy, D. S., Yashayaev, I., Proshutinsky, A., Bamber, J. L., Bashmachnikov, I. L., Chassignet, E. P., et al. (2019). Role of Greenland freshwater anomaly in the recent freshening of the subpolar North Atlantic. *Journal of Geophysical Research: Oceans*, *124*(5), 3333–3360. https://doi.org/10.1029/2018JC014686

ECCO Consortium, Fukumori, I., Wang, O., Fenty, I., Forget, G., Heimbach, P., & Ponte, R. M. (2021a). ECCO global mean sea level—Monthly mean (version 4 release 4) [Dataset]. *PO.DAAC, CA, USA*. https://doi.org/10.5067/ECTSM-MSL44

ECCO Consortium, Fukumori, I., Wang, O., Fenty, I., Forget, G., Heimbach, P., & Ponte, R. M. (2021b). Synopsis of the ECCO central production global Ocean and sea-ice state estimate, version 4 release 4. *Zenodo*. https://doi.org/10.5281/zenodo.4533349

Enderlin, E. M., Hamilton, G. S., Straneo, F., & Sutherland, D. A. (2016). Iceberg meltwater fluxes dominate the freshwater budget in Greenland's iceberg-congested glacial fjords. *Geophysical Research Letters*, *43*(21), 11287–11294. https://doi.org/10.1002/2016GL070718

Forget, G., Campin, J.-M., Heimbach, P., Hill, C. N., Ponte, R. M., & Wunsch, C. (2015). ECCO version 4: An integrated framework for non-linear inverse modeling and global ocean state estimation. *Geoscientific Model Development*, *8*(10), 3071–3104. https://doi.org/10.5194/gmd-8-3071-2015

Fox-Kemper, B., Hewitt, H., Xiao, C., Aeth algeirsdóttir, G., Drijfhout, S., Edwards, T., et al. (2021). Ocean, cryosphere and sea level change [Book Section]. In V. Masson-Delmotte, P. Zhai, A. Pirani, S. L. Connors, C. Pean, S. Berger, et al. (Eds.), *Climate change 2021: The physical science basis. Contribution of working group I to the sixth assessment report of the intergovernmental panel on climate change* (pp. 1211–1362). https://doi.org/10.1017/9781009157896.011

Fu, Y., Feng, Y., Zhou, D., & Zhou, X. (2021). Absolute sea level variability of Arctic Ocean in 1993–2018 from satellite altimetry and tide gauge observations. *Acta Oceanologica Sinica*, *40*(10), 76–83. https://doi.org/10.1007/s13131-021-1820-4

Fukumori, I., Wang, O., & Fenty, I. (2021). Causal mechanisms of sea level and freshwater content change in the Beaufort Sea. *Journal of Physical Oceanography*, *51*(10), 3217–3234. https://doi.org/10.1175/JPO-D-21-0069.1

Garcia, H., Boyer, T., Baranova, O., Locarnini, R., Mishonov, A., Grodsky, A., et al. (2019). World ocean atlas 2018: Product documentation. A. Mishonov, Technical Editor.

Giles, K. A., Laxon, S. W., Ridout, A. L., Wingham, D. J., & Bacon, S. (2012). Western Arctic Ocean freshwater storage increased by wind-driven spin-up of the Beaufort Gyre. *Nature Geoscience*, *5*(3), 194–197. https://doi.org/10.1038/ngeo1379

Gill, A. E., & Niller, P. P. (1973). The theory of the seasonal variability in the ocean. *Deep-Sea Research and Oceanographic Abstracts*, *20*(2), 141–177. https://doi.org/10.1016/0011-7471(73)90049-1

Gladish, C. V., Holland, D. M., Rosing-Asvid, A., Behrens, J. W., & Boje, J. (2015). Oceanic boundary conditions for Jakobshavn Glacier. Part I: Variability and renewal of Ilulissat Icefjord waters, 2001–14. *Journal of Physical Oceanography*, *45*(1), 3–32. https://doi.org/10.1175/JPO-D-14-0044.1

Greatbatch, R. J. (1994). A note on the representation of steric sea level in models that conserve volume rather than mass. *Journal of Geophysical Research*, *99*(C6), 12767–12771. https://doi.org/10.1029/94JC00847

Gregory, J. M., Griffies, S. M., Hughes, C. W., Lowe, J. A., Church, J. A., Fukimori, I., et al. (2019). Concepts and terminology for Sea Level: Mean, variability and change, both local and global. *Surveys in Geophysics*, *40*(6), 1251–1289. https://doi.org/10.1007/s10712-019-09525-z

Hall, S. B., Subrahmanyam, B., & Steele, M. (2023). The role of the Russian shelf in seasonal and interannual variability of Arctic Sea Surface salinity and freshwater content. *Journal of Geophysical Research: Oceans*, *128*(1), e2022JC019247. https://doi.org/10.1029/2022JC019247

Hanna, E., Jones, J. M., Cappelen, J., Mernild, S. H., Wood, L., Steffen, K., & Huybrechts, P. (2013). The influence of north Atlantic atmospheric and oceanic forcing effects on 1900–2010 Greenland summer climate and ice melt/runoff. *International Journal of Climatology*, *33*(4), 862–880. https://doi.org/10.1002/joc.3475

Held, I. M. (1983). Stationary and quasi-stationary eddies in the extratropical troposphere: Theory. In B. J. Hoskins, & R. P. Pearce, (Eds.), *Large-scale dynamical processes in the atmosphere*, Academic Press. (pp. 127–168).

Hochet, A., Lique, C., Sévellec, F., & Llovel, W. (2024). Drivers of interannual salinity variability in the Arctic Ocean. *Journal of Geophysical Research: Oceans*, *129*(6), e2023JC020852. https://doi.org/10.1029/2023jc020852

Hordoir, R., Skagseth, y., Ingvaldsen, R. B., Sandø, A. B., Löptien, U., Dietze, H., et al. (2022). Changes in arctic stratification and mixed layer depth cycle: A modeling analysis. *Journal of Geophysical Research: Oceans*, *127*(1), e2021JC017270. https://doi.org/10.1029/2021JC017270

Hurrell, J., Deser, C., & Phillips, A. (2019). North Atlantic Oscillation (NAO) [Dataset]. *Climatic Research Unit, University of East Anglia*, 447–454. https://doi.org/10.1016/b978-0-12-409548-9.11621-5

IPCC. (2021). Annex IV: Modes of variability. [cassou, c., a. cherchi, y. kosaka (eds.)] [Book Section]. In V. Masson-Delmotte (Eds.), *Climate change 2021: The physical science basis. Contribution of working group I to the sixth assessment report of the intergovernmental panel on climate change* (pp. 2153–2192). Cambridge University Press. https://doi.org/10.1017/9781009157896.018

Jahn, A., Aksenov, Y., de Cuevas, B. A., de Steur, L., Häkkinen, S., Hansen, E., et al. (2012). Arctic Ocean freshwater: How robust are model simulations? *Journal of Geophysical Research*, *117*(C8), C00D16. https://doi.org/10.1029/2012JC007907

Japan Meteorological Agency, Japan. (2013). Jra-55: Japanese 55-year reanalysis, daily 3-hourly and 6-hourly data [Dataset]. *Boulder CO: Research Data Archive at the National Center for Atmospheric Research, Computational and Information Systems Laboratory*. https://doi.org/10.5065/D6HH6H41

Jin, Y., Chen, M., Yan, H., Wang, T., & Yang, J. (2023). Sea level variation in the Arctic Ocean since 1979 based on ORAS5 data. *Frontiers in Marine Science*, *10*, 1197456. https://doi.org/10.3389/fmars.2023.1197456

Jones, P. D., Jonsson, T., & Wheeler, D. (1997). Extension to the North Atlantic oscillation using early instrumental pressure observations from Gibraltar and South-West Iceland. *International Journal of Climatology*, *17*(13), 1433–1450. https://doi.org/10.1002/(SICI)1097-0088(19971115)17:13(1433::AID-JOC203)3.0.CO;2-P

Kelly, S. J., Proshutinsky, A., Popova, E. K., Aksenov, Y. K., & Yool, A. (2019). On the origin of water masses in the Beaufort gyre. *Journal of Geophysical Research: Oceans*, *124*(7), 4696–4709. https://doi.org/10.1029/2019JC015022

Kenigson, J. S., & Timmermans, M.-L. (2021). Arctic cyclone activity and the Beaufort high. *Journal of Climate*, *34*(10), 4119–4127. https://doi.org/10.1175/JCLI-D-20-0771.1

Killworth, P. D., Chelton, D. B., & de Szoeke, R. A. (1997). The speed of observed and theoretical long extratropical planetary waves. *Journal of Physical Oceanography*, *27*(9), 1946–1966. https://doi.org/10.1175/1520-0485(1997)027<1946:tsooat>2.0.co;2

Kobayashi, S., Ota, Y., Harada, Y., Ebita, A., Moriya, M., Onoda, H., et al. (2015). The JRA-55 reanalysis: General specifications and basic characteristics. *Journal of the Meteorological Society of Japan. Ser. II*, *93*(1), 5–48. https://doi.org/10.2151/jmsj.2015-001

Kryzhov, V. N., & Gorelits, O. V. (2015). The Arctic oscillation and its impact on temperature and precipitation in Northern Eurasia in the 20th century. *Russian Meteorology and Hydrology*, *40*(11), 711–721. https://doi.org/10.3103/S1068373915110011

Lambert, E., Nummelin, A., Pemberton, P., & Ilıcak, M. (2019). Tracing the imprint of River Runoff variability on Arctic water mass transformation. *Journal of Geophysical Research: Oceans*, *124*(1), 302–319. https://doi.org/10.1029/2017JC013704

Large, W., & Yeager, S. (2004). Diurnal to decadal global forcing for ocean and sea-ice models the data sets and flux climatologies (Tech. Rep.). *UCAR/NCAR*. https://doi.org/10.5065/D6KK98Q6

Liu, Z. (1999). Planetary wave modes in the thermocline: Non-Doppler-shift mode, advective mode and green mode. *Quarterly Journal of the Royal Meteorological Society*, *125*(556), 1315–1339. https://doi.org/10.1002/qj.1999.49712555611

Llovel, W., Balem, K., Tajouri, S., & Hochet, A. (2023). Cause of substantial global mean sea level rise over 2014–2016. *Geophysical Research Letters*, *50*(19), e2023GL104709. https://doi.org/10.1029/2023GL104709

Lorbacher, K., Dengg, J., Böning, C. W., & Biastoch, A. (2010). Regional patterns of sea level change related to interannual variability and multidecadal trends in the Atlantic meridional overturning circulation. *Journal of Climate*, *23*(15), 4243–4254. https://doi.org/10.1175/2010JCLI3341.1

Losch, M., Menemenlis, D., Campin, J.-M., Heimbach, P., & Hill, C. (2010). On the formulation of sea-ice models. Part 1: Effects of different solver implementations and parameterizations. *Ocean Modelling*, *33*(1), 129–144. https://doi.org/10.1016/j.ocemod.2009.12.008

Ludwigsen, C. B., Andersen, O. B., & Rose, S. K. (2022). Components of 21 years (1995–2015) of absolute sea level trends in the Arctic. *Ocean Science*, *18*(1), 109–127. https://doi.org/10.5194/os-18-109-2022

Lyu, G., Serra, N., Zhou, M., & Stammer, D. (2022). Arctic sea level variability from high-resolution model simulations and implications for the Arctic observing system. *Ocean Science*, *18*(1), 51–66. https://doi.org/10.5194/os-18-51-2022

Madec, G., Bourdallé-Badie, R., Chanut, J., Clementi, E., Coward, A., Ethé, C., et al. (2019). Nemo ocean engine. *Zenodo*. https://doi.org/10.5281/zenodo.3878122

Manucharyan, G. E., & Spall, M. A. (2016). Wind-driven freshwater buildup and release in the Beaufort gyre constrained by mesoscale eddies. *Geophysical Research Letters*, *43*(1), 273–282. https://doi.org/10.1002/2015GL065957

Manucharyan, G. E., Spall, M. A., & Thompson, A. F. (2016). A theory of the wind-driven Beaufort gyre variability. *Journal of Physical Oceanography*, *46*(11), 3263–3278. https://doi.org/10.1175/JPO-D-16-0091.1

Marsh, R., Desbruyères, D., Bamber, J. L., de Cuevas, B. A., Coward, A. C., & Aksenov, Y. (2010). Short-term impacts of enhanced Greenland freshwater fluxes in an eddy-permitting ocean model. *Ocean Science*, *6*(3), 749–760. https://doi.org/10.5194/os-6-749-2010

Marsh, R., Ivchenko, V. O., Skliris, N., Alderson, S., Bigg, G. R., Madec, G., et al. (2015). NEMO–ICB (V1.0): Interactive icebergs in the nemo ocean model globally configured at eddy-permitting resolution. *Geoscientific Model Development*, *8*(5), 1547–1562. https://doi.org/10.5194/gmd-8-1547-2015

Marshall, J., Adcroft, A., Hill, C., Perelman, L., & Heisey, C. (1997). A finite-volume, incompressible Navier Stokes model for studies of the ocean on parallel computers. *Journal of Geophysical Research*, *102*(C3), 5753–5766. https://doi.org/10.1029/96JC02775

Moftakhari, H. R., AghaKouchak, A., Sanders, B. F., Feldman, D. L., Sweet, W., Matthew, R. A., & Luke, A. (2015). Increased nuisance flooding along the coasts of the United States due to sea level rise: Past and future. *Geophysical Research Letters*, *42*(22), 9846–9852. https://doi.org/10.1002/2015GL066072

Molines, J.-M., & Leroux, S. (2024). imhotep-project/simus-imhotep: Config Imhotep for Tajouri et Al. 2024 paper [Software]. *Zenodo*. https://doi.org/10.5281/zenodo.13327839

Moon, T., Sutherland, D. A., Carroll, D., Felikson, D., Kehrl, L., & Straneo, F. (2018). Subsurface iceberg melt key to Greenland fjord freshwater budget. *Nature Geoscience*, *11*(1), 49–54. https://doi.org/10.1038/s41561-017-0018-z

Morison, J., Kwok, R., Dickinson, S., Andersen, R., Peralta-Ferriz, C., Morison, D., et al. (2021). The cyclonic mode of Arctic Ocean circulation. *Journal of Physical Oceanography*, *51*(4), 1053–1075. https://doi.org/10.1175/JPO-D-20-0190.1

Morison, J., Kwok, R., Peralta-Ferriz, C., Alkire, M., Rigor, I., Andersen, R., & Steele, M. (2012). Changing Arctic Ocean freshwater pathways. *Nature*, *481*(7379), 66–70. https://doi.org/10.1038/nature10705

Moritz, R. E., Bitz, C. M., & Steig, E. J. (2002). Dynamics of recent climate change in the Arctic. *Science*, *297*(5586), 1497–1502. https://doi.org/10.1126/science.1076522

Mouginot, J., Rignot, E., Bjørk, A. A., van den Broeke, M., Millan, R., Morlighem, M., et al. (2019). Forty-six years of Greenland Ice Sheet mass balance from 1972 to 2018. *Proceedings of the National Academy of Sciences*, *116*(19), 9239–9244. https://doi.org/10.1073/pnas.1904242116

Moyer, A. N., Sutherland, D. A., Nienow, P. W., & Sole, A. J. (2019). Seasonal variations in iceberg freshwater flux in Sermilik Fjord, Southeast Greenland from sentinel-2 imagery. *Geophysical Research Letters*, *46*(15), 8903–8912. https://doi.org/10.1029/2019GL082309

Nerem, R. S., Beckley, B. D., Fasullo, J. T., Hamlington, B. D., Masters, D., & Mitchum, G. T. (2018). Climate-change–driven accelerated sea-level rise detected in the altimeter era. *Proceedings of the National Academy of Sciences*, *115*(9), 2022–2025. https://doi.org/10.1073/pnas.1717312115

Neumann, B., Vafeidis, A. T., Zimmermann, J., & Nicholls, R. J. (2015). Future coastal population growth and exposure to seasea-level rise and coastal flooding—A global assessment. *PLoS One*, *10*(3), 1–34. https://doi.org/10.1371/journal.pone.0118571

Nummelin, A., Ilicak, M., Li, C., & Smedsrud, L. H. (2016). Consequences of future increased Arctic runoff on Arctic Ocean stratification, circulation, and sea ice cover. *Journal of Geophysical Research: Oceans*, *121*(1), 617–637. https://doi.org/10.1002/2015JC011156

Nygård, T., Naakka, T., & Vihma, T. (2020). Horizontal moisture transport dominates the regional moistening patterns in the Arctic. *Journal of Climate*, *33*(16), 6793–6807. https://doi.org/10.1175/JCLI-D-19-0891.1

Piecuch, C. G., & Wadehra, R. (2020). Dynamic Sea level variability due to seasonal river discharge: A preliminary global ocean model study. *Geophysical Research Letters*, *47*(4), e2020GL086984. https://doi.org/10.1029/2020GL086984

Prandi, P., Poisson, J.-C., Faugère, Y., Guillot, A., & Dibarboure, G. (2021). Arctic sea surface height maps from multi-altimeter combination. *Earth System Science Data*, *13*(12), 5469–5482. https://doi.org/10.5194/essd-13-5469-2021

Prandi, P., & Veillard, P. (2020). Arctic Ocean gridded and along-track sea level anomaly maps [Dataset]. *CNES*. https://doi.org/10.24400/527896/A01-2020.001

Proshutinsky, A., Ashik, I. M., Dvorkin, E. N., Häkkinen, S., Krishfield, R. A., & Peltier, W. R. (2004). Secular sea level change in the Russian sector of the Arctic Ocean. *Journal of Geophysical Research*, *109*(C3), C03042. https://doi.org/10.1029/2003JC002007

Proshutinsky, A., Dukhovskoy, D., Timmermans, M.-L., Krishfield, R., & Bamber, J. L. (2015). Arctic circulation regimes. *Philosophical Transactions of the Royal Society A: Mathematical, Physical & Engineering Sciences*, *373*(2052), 20140160. https://doi.org/10.1098/rsta.2014.0160

Proshutinsky, A., Krishfield, R., Timmermans, M.-L., Toole, J., Carmack, E., McLaughlin, F., et al. (2009). Beaufort Gyre freshwater reservoir: State and variability from observations. *Journal of Geophysical Research*, *114*(C1), C00A10. https://doi.org/10.1029/2008JC005104

Proshutinsky, A., Krishfield, R., Toole, J. M., Timmermans, M., Williams, W., Zimmermann, S., et al. (2019). Analysis of the Beaufort gyre freshwater content in 2003–2018. *Journal of Geophysical Research: Oceans*, *124*(12), 9658–9689. https://doi.org/10.1029/2019JC015281

Raj, R. P., Andersen, O. B., Johannessen, J. A., Gutknecht, B. D., Chatterjee, S., Rose, S. K., et al. (2020). Arctic Sea level budget assessment during the GRACE/Argo time period. *Remote Sensing*, *12*(17), 2837. https://doi.org/10.3390/rs12172837

Regan, H. C., Lique, C., & Armitage, T. W. K. (2019). The Beaufort gyre extent, shape, and location between 2003 and 2014 from satellite observations. *Journal of Geophysical Research: Oceans*, *124*(2), 844–862. https://doi.org/10.1029/2018JC014379

Rignot, E., Jacobs, S., Mouginot, J., & Scheuchl, B. (2013). Ice-shelf melting around Antarctica. *Science*, *341*(6143), 266–270. https://doi.org/10.1126/science.1235798

Rose, S. K., Andersen, O. B., Passaro, M., Ludwigsen, C. A., & Schwatke, C. (2019). Arctic Ocean Sea Level record from the complete Radar altimetry era: 1991–2018. *Remote Sensing*, *11*(14), 1672. https://doi.org/10.3390/rs11141672

Rossby, C. G. (1939). Relation between variations in the intensity of the zonal circulation of the atmosphere and the displacements of the semi-permanent centers of action. *Journal of Marine Research*, *2*(1), 38–55. https://doi.org/10.1357/002224039806649023

Solomon, A., Heuzé, C., Rabe, B., Bacon, S., Bertino, L., Heimbach, P., et al. (2021). Freshwater in the Arctic ocean 2010–2019. *Ocean Science*, *17*(4), 1081–1102. https://doi.org/10.5194/os-17-1081-2021

Stammer, D. (2008). Response of the global ocean to Greenland and Antarctic ice melting. *Journal of Geophysical Research*, *113*(C6), C06022. https://doi.org/10.1029/2006JC004079

Stammer, D., Cazenave, A., Ponte, R. M., & Tamisiea, M. E. (2013). Causes for contemporary regional Sea Level changes. *Annual Review of Marine Science*, *5*(1), 21–46. https://doi.org/10.1146/annurev-marine-121211-172406

Stephenson, D., & Sévellec, F. (2021). The active and passive roles of the ocean in generating basin-scale heat content variability. *Geophysical Research Letters*, *48*(19), e2020GL091874. https://doi.org/10.1029/2020GL091874

Straneo, F., & Heimbach, P. (2013). North Atlantic warming and the retreat of Greenland's outlet glaciers. *Nature*, *504*(7478), 36–43. https://doi.org/10.1038/nature12854

Straneo, F., Heimbach, P., Sergienko, O., Hamilton, G., Catania, G., Griffies, S., et al. (2013). Challenges to understanding the dynamic response of Greenland's marine terminating glaciers to oceanic and atmospheric forcing. *Bulletin of the American Meteorological Society*, *94*(8), 1131–1144. https://doi.org/10.1175/BAMS-D-12-00100.1

Suzuki, T., Yamazaki, D., Tsujino, H., Komuro, Y., Nakano, H., & Urakawa, S. (2018). A dataset of continental river discharge based on JRA-55 for use in a global ocean circulation model. *Journal of Oceanography*, *74*(4), 421–429. https://doi.org/10.1007/s10872-017-0458-5

Swingedouw, D., Rodehacke, C. B., Behrens, E., Menary, M., Olsen, S. M., Gao, Y., et al. (2013). Decadal fingerprints of freshwater discharge around Greenland in a multi-model ensemble. *Climate Dynamics*, *41*(3), 695–720. https://doi.org/10.1007/s00382-012-1479-9

Tajouri, S. (2024). stajouri/noteboooks_sla_bgr: Sla_beaufort_gyre [ComputationalNotebook]. *Zenodo*. https://doi.org/10.5281/zenodo.13332648

Timmermans, M., & Marshall, J. (2020). Understanding Arctic Ocean circulation: A review of ocean dynamics in a changing climate. *Journal of Geophysical Research: Oceans*, *125*(4), e2018JC014378. https://doi.org/10.1029/2018JC014378

Timmermans, M.-L., & Toole, J. M. (2023). The Arctic Ocean's Beaufort gyre. *Annual Review of Marine Science*, *15*(1), 223–248. https://doi.org/10.1146/annurev-marine-032122-012034

Vancoppenolle, M., Rousset, C., Blockley, E., Aksenov, Y., Feltham, D., Fichefet, T., et al. (2023). SI3, the nemo sea ice engine. *Zenodo*. https://doi.org/10.5281/zenodo.7534900

Vihma, T., Screen, J., Tjernström, M., Newton, B., Zhang, X., Popova, V., et al. (2016). The atmospheric role in the arctic water cycle: A review on processes, past and future changes, and their impacts. *Journal of Geophysical Research: Biogeosciences*, *121*(3), 586–620. https://doi.org/10.1002/2015JG003132

Villamil-Otero, G. A., Zhang, J., He, J., & Zhang, X. (2018). Role of extratropical cyclones in the recently observed increase in poleward moisture transport into the Arctic Ocean. *Advances in Atmospheric Sciences*, *35*(1), 85–94. https://doi.org/10.1007/s00376-017-7116-0

Zhang, X., He, J., Zhang, J., Polyakov, I., Gerdes, R., Inoue, J., & Wu, P. (2013). Enhanced poleward moisture transport and amplified northern high-latitude wetting trend. *Nature Climate Change*, *3*(1), 47–51. https://doi.org/10.1038/nclimate1631

References From the Supporting Information

Gilbert, E., & Kittel, C. (2021). Surface melt and runoff on Antarctic ice shelves at 1.5°C, 2°C, and 4°C of future warming. *Geophysical Research Letters*, *48*(8), e2020GL091733. https://doi.org/10.1029/2020GL091733

Joughin, I., Tulaczyk, S., Bamber, J. L., Blankenship, D., Holt, J. W., Scambos, T., & Vaughan, D. G. (2009). Basal conditions for pine island and Thwaites glaciers, West Antarctica, determined using satellite and airborne data. *Journal of Glaciology*, *55*(190), 245–257. https://doi.org/10.3189/002214309788608705

Mathiot, P., & Jourdain, N. C. (2023). High-end projections of southern ocean warming and Antarctic ice shelf melting in conditions typical of the end of the 23rd century. *EGUsphere*, *2023*, 1–27. https://doi.org/10.5194/egusphere-2023-1606

Mathiot, P., Jenkins, A., Harris, C., & Madec, G. (2017). Explicit representation and parametrised impacts of under ice shelf seas in the z^* coordinate ocean model nemo 3.6. *Geoscientific Model Development*, *10*(7), 2849–2874. https://doi.org/10.5194/gmd-10-2849-2017